H. U. Levatti,[1] P. C. Prat,[2] A. Ledesma,[3] A. Cuadrado,[4] and J. A. Cordero[5]

# Experimental Analysis of 3D Cracking in Drying Soils Using Ground-Penetrating Radar

**Geotechnical Testing Journal**

H. U. Levatti,[1] P. C. Prat,[2] A. Ledesma,[3] A. Cuadrado,[4] and J. A. Cordero[5]          1  AQ1

# Experimental Analysis of 3D Cracking in Drying Soils Using Ground-Penetrating Radar

## Reference

[1] College of Engineering, Swansea University, Bay Campus, Swansea SA1 8EN, United Kingdom; formerly of Dept. of Civil and Environmental Engineering, Technical University of Catalonia (UPC-BarcelonaTech), 08034 Barcelona, Spain, e-mail: h.u.levatti@swansea.ac.uk

[2] Dept. of Civil and Environmental Engineering, Technical University of Catalonia (UPC-BarcelonaTech), Room D2-202b, Jordi Girona 1-3, Edifici D2, 08034 Barcelona, Spain, e-mail: pere.prat@upc.edu

[3] Dept. of Civil and Environmental Engineering, Technical University of Catalonia (UPC-BarcelonaTech), Jordi Girona 1-3, Edifici D2, Room D2-209, 08034 Barcelona, Spain, e-mail: alberto.ledesma@upc.edu

[4] Dept. of Civil and Environmental Engineering, Technical University of Catalonia (UPC-BarcelonaTech), Room D2-214, Jordi Girona 1-3, Edifici D2, 08034 Barcelona, Spain, e-mail: agustin.cuadrado@upc.edu

[5] Dept. of Civil and Environmental Engineering, Technical University of Catalonia (UPC-BarcelonaTech), Room D2-215, Jordi Girona 1-3, Edifici D2, 08034 Barcelona, Spain, e-mail: josbel.andreina.cordero@upc.edu

AQ2

## ABSTRACT

This paper describes the capabilities of a novel technique to investigate crack formation and propagation in drying soils. The technique is a relatively simple, non-destructive indirect technique using a ground-penetrating-radar (GPR) system to detect cracks that form and propagate inside a soil specimen during desiccation. Although GPR devices have been used for multiple applications, their use in soils for the detection of small desiccation cracks has not been demonstrated yet. The experiment and the methodology used to test the accuracy of a small compact commercial GPR device for crack identification are described. The main objective was to identify what type of signals and what crack width and separation between them can be detected using the GPR device. The results indicate that cracks of 1 or 2 mm wide can be detected depending on its position and shape, whereas sub-millimeter cracks are undetectable with the currently existing devices in the market. Regardless of this limitation, the GPR method can be useful to find time-related bounds of when the cracks appear, to point at their location and sometimes at the separation between two of them. Detection of cracks with origin at the bottom or within the specimen was accomplished with this system. Distances of 5 cm or more between cracks can be detected and measured, as well, with accuracy.

## Keywords

desiccation cracks, auscultation, ground-penetrating radar

# Introduction

Soils made of clay or silt tend to shrink and crack when subjected to desiccation. The drying process is very complex in soils and includes physical, chemical, hydraulic, and mechanical phenomena. The crack patterns are unique and its development depends on many factors. From the experimental point of view, several authors have studied this process since the early twentieth century (Haines 1923; Longwell 1928; Simpson 1936; Jahn 1950; Knechtel 1952; Skempton and Northey 1952; Lachenbruch 1961; White 1961; Willden and Mabey 1961) and many significant contributions have been made in the last half century (Corte and Higashi 1960; Lau 1987; Morris et al. 1992; Kodikara et al. 2000, 2004; Chertkov 2002; Ávila 2004; Vogel et al. 2005; Nahlawi and Kodikara 2006; Rodríguez et al. 2007; Hu et al. 2008; Lakshmikantha 2009; Lakshmikantha et al. 2009, 2012, 2013b; Péron et al. 2009; Tang et al. 2011). However, until the development of unsaturated soil mechanics the problem has not been analyzed considering the parameters that govern the behavior of soil in the unsaturated state, primarily suction. Tensile strength (suction dependent) and fracture toughness are shown as the most relevant parameters (Ávila 2004; Lakshmikantha et al. 2012), but a definite model explaining that process is yet to be formulated.

In laboratory tests, many cracks appear on the top boundary of soil specimens. However, there are others that are not visible, and several experiments have shown that cracks may start at any point within the specimen (Lakshmikantha et al. 2009, 2013a, 2016; Levatti 2015). To detect the cracks that start at the bottom boundary or within the sample one would need sophisticated techniques such as X-ray, magnetic resonance, or electrical resistivity tomography (Samouëlian et al. 2003; Otani and Obara 2004; Mukunoki et al. 2010; Hassan and Toll 2013), usually very expensive and involving very complicated setups. However, detection of those non-visible cracks is important because cracking because of drying in soils is a very complex three-dimensional process and the study cannot limit itself to the outer visible cracks.

This paper presents a relatively simple, non-destructive, indirect technique using a ground-penetrating radar (GPR) device to detect cracks that form and propagate within the specimen during desiccation (Prat et al. 2013; Cordero et al. 2014; Levatti 2015). Whereas continuous monitoring of surface cracking allows following the evolution of the external cracking pattern with time, the GPR technique may be helpful to detect the cracks within the soil, giving a more complete picture of the phenomenon with greater accuracy.

The main objective of this work is to identify what type of signals, and what crack width and separation can be detected using a small commercial GPR device. The ability to detect cracks which initiate at the bottom or inside the soil mass and appear later on the top of the specimen needed also to be demonstrated. The results indicate that cracks of one or two millimeters wide can be detected depending on its position and shape. Separations of 5 cm or more are easily detected and can be measured with accuracy. On the other hand, sub-millimeter cracks are undetectable with the currently existing devices in the market. The proposed method can also be useful to estimate when and where the cracks initiate with sufficient accuracy.

## BASIC PRINCIPLES OF A GROUND-PENETRATING RADAR SYSTEM

The GPR is a non-destructive technique that uses electromagnetic pulses to detect reflecting surfaces inside the soil allowing imaging of buried objects, stratigraphy, and other soil features at shallow depths, providing continuous, real-time profiles, of the subsurface. The equipment consists of a computerized control system connected to antennas that are moved slowly along a predefined path on the ground surface to produce a continuous subsurface profile. One antenna emits the electromagnetic pulses and a second one records the reflected signals from the objects, discontinuities, or other features inside the soil. The reflected wave originates from changes in the electromagnetic properties of the soil that may be caused by variations in water content, density changes because of the presence of stratigraphic surfaces, and discontinuities or voids existing in the path of the pulse. Therefore, the success of the technique relies, to a great extent, on a sufficient dielectric contrast at the crack location to produce a clear reflected signal. The penetration depth of the pulses, and data resolution, depend on the wavelength and the soil's dielectric constant. These parameters are mainly controlled by the soil's moisture content. The depth and resolution are inversely proportional magnitudes; increasing the antenna's frequency, a better resolution is obtained but the depth is smaller.

The theoretical background of the method is the theory of electromagnetic fields, described by Maxwell's equations (1), and the constitutive equations (2):

$$\nabla D = \rho_f; \quad \nabla B = 0; \quad \nabla \times E = -\frac{\partial B}{\partial t} + M;$$
$$\nabla \times H = -\frac{\partial D}{\partial t} + J \tag{1}$$

$$D = \varepsilon E; \quad H = \frac{B}{\mu}; \quad J = \sigma E \tag{2}$$

where:

$E$ = electric field,
$H$ = magnetic field,
$D$ = electric displacement field,
$B$ = magnetic induction,
$J$ = free current density,
$M$ = magnetization field, and
$\rho_f$ = free charge density.

**TABLE 1** Electromagnetic parameters and wave propagation characteristics in air and water.

| Material | $\varepsilon_r$ | $\sigma$(mS/m) | $\mu_r$ | $v$(cm/ns) | $\Gamma$(dB/m) |
|---|---|---|---|---|---|
| Air | 1 | 0 | 1.0003 | 30 | 0 |
| Distilled water | – | 0.01 | – | – | 0.002 |
| Freshwater | 80–81 | 0.1–10 | 1 | 3.3 | 0.1–0.18 |
| Seawater | 81–88 | 4000 | – | – | 330–1000 |
| Polar snow | 1.4–3.0 | – | 1 | 19.4–25.2 | – |
| Polar ice | 3.00–3.15 | 0.02–0.003 | – | 16.8 | 0.01 |
| Tempered ice | 3.2 | $5.10^{-4}$–$8.10^{-6}$ | – | 16.7 | 0.01 |
| Pure ice | 3.2 | – | – | 16.7 | 0.01 |
| Freshwater lake ice | 4 | – | – | 15 | 0.01 |
| Sea ice | 2.5–8.0 | – | – | 7.8–15.7 | – |
| Permafrost | 1–8 | 1.0–0.1 | 1 | 10.6–30.0 | – |

The parameters that appear in Eq 2 describe the electromagnetic properties of the medium and are $\varepsilon$ (dielectric permittivity), $\mu$ (magnetic permeability), and $\sigma$ (electric conductivity).

The principle of a GPR is based on the dielectric permittivity, $\varepsilon$ in Eq 2, which represents the permittivity of an electromagnetic pulse through the medium, compared to the void permittivity. It is a constant that gives a measure of the polarizing ability of a material in the presence of an electric field. This parameter is defined as the ratio of the capacitance of parallel plate electrodes containing dielectric material to the capacitance in a vacuum. The value provides an indication of the static response of the material when in the presence of an external electric field, i.e., describes how an electric field affects and is affected by the material. It is a non-dimensional parameter that depends on the electric conductivity and the thickness of the layer. For most of the components of the soil this parameter has a value between 1 (for air) and 80 (for water). The GPR produces results by detecting wave reflections produced while the wave crosses the boundary between two materials with different dielectric constant.

The magnetic permeability, $\mu$ in Eq 2 is associated with the magnetic induction of the magnetic field intensity. It measures the degree of magnetization that a material obtains in response to an applied magnetic field. The magnetic permeability of the soil's constituents is close to 1 (provided they are not ferromagnetic materials), independent of the frequency of the magnetic field. Therefore, this magnitude usually has no great influence and is assumed to be constant.

The electrical conductivity, $\sigma$ in Eq 2, provides a measure of the response of the free charges existing in the material when in the presence of an external electric field. It is a material property that expresses the proportionality between the electric field applied and the electric current because of the movement of the free charges, and provides a measure of the ability of a material to conduct an electric current, according to Ohm's law in Eq 2.

The majority of soils and rocks that form the Earth's crust are composed of silicate minerals, which are electrical insulators (Morrison and Gasperikova 2015). Electrical currents in these materials can only be carried by ions within the fluids filling the pores between the minerals. In that case, the conductivity depends mainly on the water content and on the chemical composition of the salts dissolved in the pore water. On the other hand, some materials such as metallic ore minerals or graphite are electrical conductors or semiconductors in which the electric current is carried by electrons. Except in this latter case, for most rocks and soils where current is carried by ions in the pore fluid, the conductivity depends on the porosity, salt concentration in the pore fluid, temperature, degree of saturation, pressure, and clay content. In general, the conductivity increases

**TABLE 2** Electromagnetic properties of soil components: Dielectric constant ($k$); electrical conductivity ($\sigma$); propagation velocity ($v$); and attenuation coefficient ($\alpha$).

| Material | $k$ | $\sigma$(mS/m) | $v$(m/ns) | $\alpha$(dB/m) |
|---|---|---|---|---|
| Air | 1 | 0 | 0.3 | 0 |
| Distilled water | 80 | 0.01 | 0.033 | 2000 |
| Fresh water | 80 | 0.5 | 0.033 | 0.1 |
| Seawater | 80 | 3000 | 0.01 | 103 |
| Dry sand | 3–5 | 0.01 | 0.15 | 0.01 |
| Saturated sand | 20–30 | 0.1–1.0 | 0.06 | 0.03–0.30 |
| Siltstone | 4–8 | 0.5–2.0 | 0.12 | 0.4–1.0 |
| Shale | 5–15 | 1–100 | 0.09 | 1–100 |
| Silt | 5–30 | 1–100 | 0.07 | 1–100 |
| Clay | 5–40 | 2–1000 | 0.06 | 1–300 |
| Granite | 4–8 | 0.01–1.00 | 0.13 | 0.01–1.00 |
| Dry salt | 5–6 | 0.01–1.00 | 0.13 | 0.01–1.00 |
| Ice | 3–4 | 0.01 | 0.16 | 0.01 |



**FIG. 1** The GSSI StructureScan Mini device.

4       *Geotechnical Testing Journal*

**TABLE 3**   Technical specifications of the StructureScan Mini device.

| Center Frequency | 1600 MHz |
|---|---|
| Depth range | <50 cm |
| Unit weight | 1.6 kg |
| Dimensions | 152 × 178 × 229 (mm) |

with water content, concentration of salts, porosity, and clay content.

Because electric currents (electromagnetic waves in general) propagate through the pore water in soils, it is important to discuss the behavior of such electromagnetic waves in the water in which they propagate at very low speed and with high attenuation. Water has a high effective dielectric permittivity, and the large contrast with the dielectric permittivity of the other soil components significantly influences the average speed of propagation of the electromagnetic waves. Studies have shown that within normal frequencies in prospecting subsurface radar, the relative dielectric permittivity and electric conductivity of the medium increases with the degree of saturation (Knoll and Knight 1994).

The presence of fine-grained material, such as clay in the soils, plays an important role in increasing its electric conductivity and dielectric permittivity. Because of atomic substitution, the clay particles are not electrically neuter, but have a net negative charge, therefore attracting cations to its surface from the surrounding fluid solution. The electrically charged particle surface plus the surrounding zone of decreasing cation

concentration (double layer) has a higher conductivity than the pore water, providing an additional path for electrical currents along the surface of the mineral particles which increases both conductivity and dielectric permittivity (Mitchell 1993; Brandes 2005).

The electromagnetic parameters of the soil are also strongly dependent on the porosity. For a dry soil, a higher percentage of pores reduces the value of both conductivity and dielectric permittivity. However, if the soil is wet the effect is not as clear, and if the soil is fully saturated then the effect is reversed.

Soils are mixtures of different types of materials, each with its own electromagnetic properties. The overall electromagnetic properties of the soil depend on the properties of each constituent and its percentage in the mixture. Several models in the literature (Pérez 2001) can be used to estimate the value of the electromagnetic properties of the soil as a function of its porosity, water content, and composition (mineral type and percentage). Using these models, it can be seen that for a single-component material and for a given porosity, the range of variation of the electromagnetic properties depends greatly on the degree of saturation, and that the range increases with increasing porosity. All of this indicates that the porosity and the fluid contained in the pores greatly influences the fluctuations of the electromagnetic properties, in particular of the relative permittivity and the electrical conductivity of the material. The pore fluid, in particular, is the main component controlling the

**FIG. 3**   Specimen and PMMA plate with grid to guide the device.



**FIG. 2**   Block test: (a) mold with strips inserted; (b) after pouring slurry; (c) surface cracks at 30 days; and (d) GPR profile shortly after the first cracks were visible on the external surface.
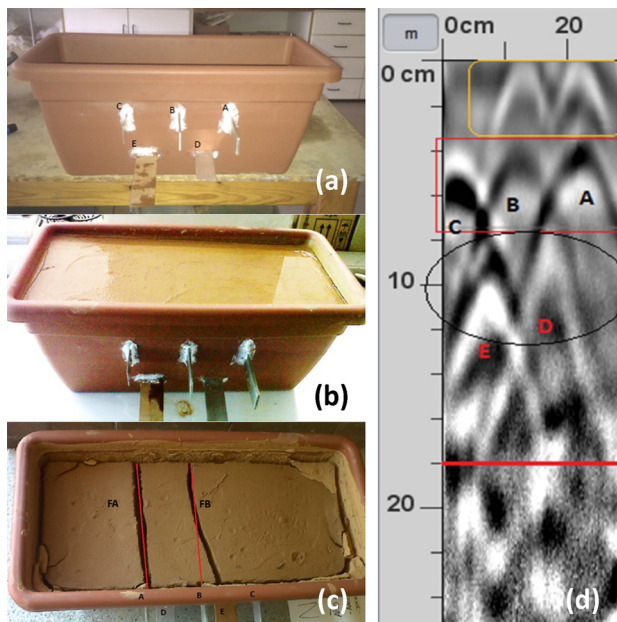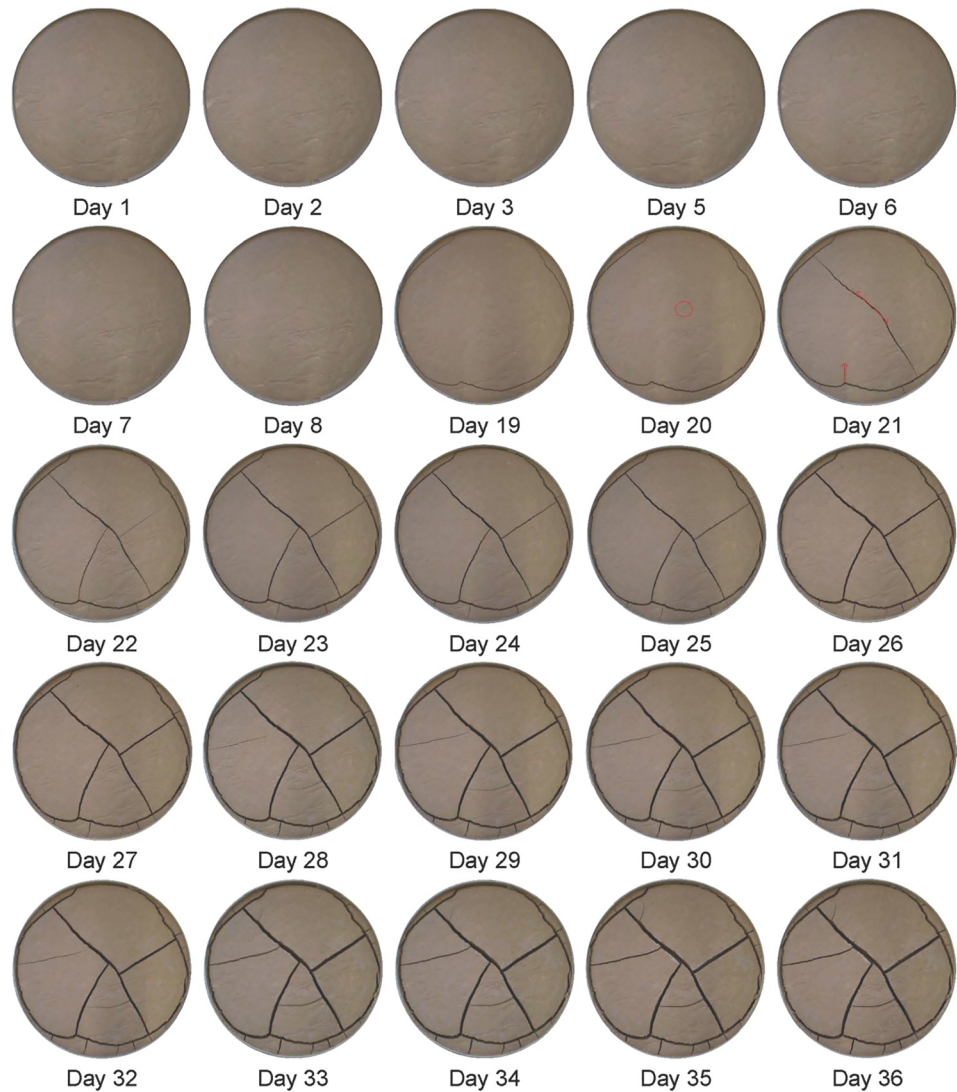
**FIG. 4**

Evolution of the specimen surface during 36 days of desiccation.



values of the overall electromagnetic properties of the material. Because the ground is formed by three distinct phases (water, gas, and solid) during the drying process, and the changes in time of each phase modify the soil's electromagnetic properties, there is added difficulty to the interpretation of the results.

Table 1 shows the electromagnetic properties of air and water under different states. Table 2 shows the electromagnetic properties of some soil constituents. This table shows the high variability of the dielectric constant and electrical conductivity, which depends largely on the constituent characteristics.

## EXPERIMENTAL PROGRAM

The soil used for the tests is a red clay that has been characterized and studied repeatedly in previous works (Barrera 2002; Lakshmikantha et al. 2006; Lakshmikantha 2009) so its geological and mineralogical composition and its hydro-mechanical behavior are well known (Barrera 2002).

To study cracking under drying conditions, it appears necessary to monitor the cracking events that occur within the soil mass, so that internal cracks can be detected before they appear on the surface and become visible. This problem is a purely three-dimensional process and it is very difficult to carry out tests that monitor those 3D cracks. For that, one could resort to techniques such as X-ray radiography, magnetic resonance imaging (MRI) or computed tomography (CT) scans. All these techniques involve very sophisticated equipment, which is very expensive and that requires tightly controlled installations and environments to avoid leakage of radiation and contamination to avoid posing a health hazard to equipment operators or visitors. This type of equipment is commonly found in health facilities and hospitals to where it would be complicated to take

6    *Geotechnical Testing Journal*



**FIG. 5**

Evolution of a sample profile at days 1, 8, 15, 22, and 29.
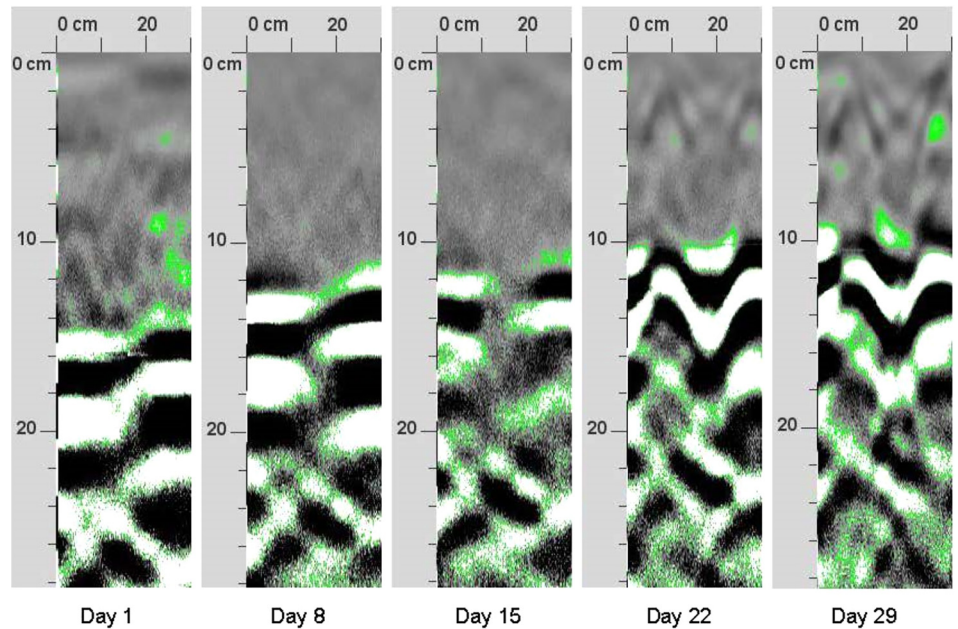
specimens in a regular basis or for long periods of time. Buying such equipment for the sole purpose of the tests object of this paper would be, of course, out of the question because of the cost.

The use of ground-penetrating radar proposed in this paper has a much lower cost, therefore, making it possible to acquire dedicated equipment for the tests. The technique has gained acceptance in recent years for subsurface imaging in geotechnical engineering and other civil engineering areas such as in detecting reinforcement bars in concrete structures or non-visible pipes in the ground or embedded in structures.

The GPR system that has been used in this work consists of a compact device (GSSI StructureScan Mini, **Fig. 1**) that includes two antennas (emitting and receiving), data-logger, basic software for in situ post-processing and a control screen for setup and management. Three laser beams are located at the bottom of the device to allow following predetermined paths with sufficient precision (**Fig. 1**).

**Table 3** shows the main technical specification of the device. The objectives of the tests described in this paper were mainly two: to detect and characterize the 3D cracking pattern inside the soil mass, and to determine the system's capabilities and

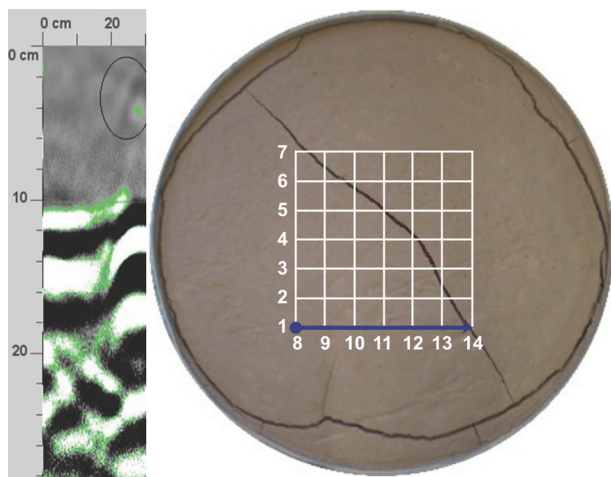**FIG. 6**    GPR profile on path 1—day 21 of desiccation test.



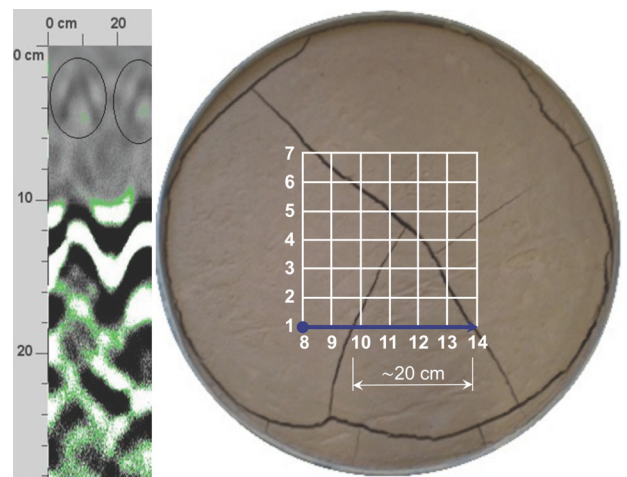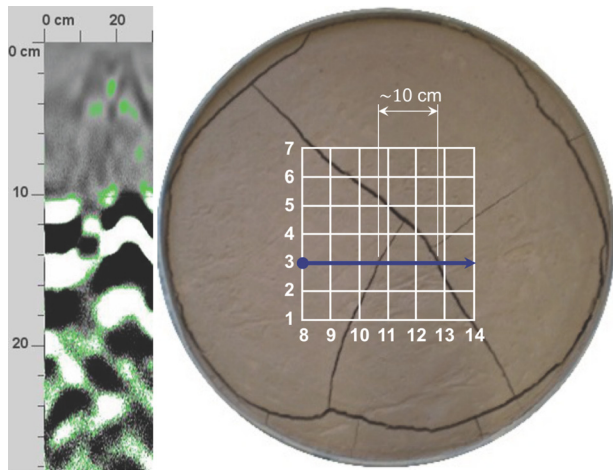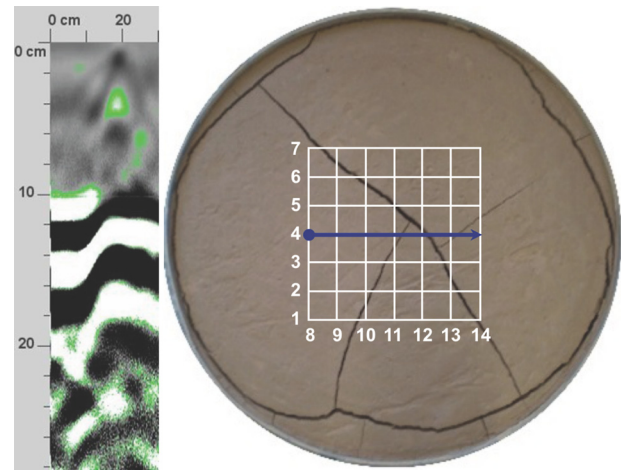**FIG. 7**    GPR profile on path 1—day 22 of desiccation test.

**FIG. 8**   GPR profile on path 3—day 22 of desiccation test.



**FIG. 9**   GPR profile on path 4—day 22 of desiccation test.

limitations regarding its ability to detect cracks, which develop within the soil mass and that therefore are not visible. The first objective can be achieved by a thorough post-processing of the data collected by the device using suitable software with the methodology developed by the authors (Prat et al. 2013). The second objective requires comparing the results of the post-processing with the external, visible cracks that will allow for calibration of the device's capabilities.

The experimental program consisted of three series of tests: (a) some preliminary tests in which the purpose was to determine the minimum crack opening that the device can detect and the influence of the orientation of the crack plane; (b) drying tests in which the specimen was dried at constant environmental conditions with the purpose of detecting internal cracks and checking the system capabilities and limitations; and (c) cyclic tests in which the specimen was subjected to drying/wetting cycles to investigate the effect of cycles in the crack pattern and for which the GPR device was used at some points during the test.

**BLOCK SPECIMEN TESTS**

The first type of tests was conducted on specimens made using a rectangular planter pot, of the type commonly found in garden stores. The specimen shape allowed the use of less amount of soil for the required specimen depth. The purpose was to determine the minimum crack opening that the GPR device can detect. Several artificial cracks were induced in the specimen using five strips of different thickness and material that were inserted into the soil (**Fig. 2a**), three vertical (A, metal, 6 mm; B, metal, 4 mm; and C, metal, 2 mm) and two horizontal (D, metal, 2 mm; and E, wood, 5 mm). After the strips were inserted in the mold the slurry was poured and left to dry in an open-air environment (**Fig. 2b**). After 1 month of drying, some cracks had appeared on the surface (**Fig. 2c**) and the consistency of the

specimen was hard enough to perform the GPR scan. This was conducted, without removing the strips, in the direction parallel to the longest side of the specimen (from right to left in the figure).

**Fig. 2d** shows the GPR profile obtained shortly after the surface cracks became visible and before the strips were removed. The figure has a rounded rectangular box on top showing two diffraction patterns shaped as hyperbolas that indicate the position of the two surface cracks. Below is a squared rectangular box showing the location of the vertical strips (A, B, C) with three consecutive hyperbolas located approximately at the same depth. In the same figure an ellipse indicates the position of strips D and E. It is not clear whether the corresponding hyperbolas have been really detected by the GPR or they are actually an overlap effect of the tail of the hyperbolas corresponding to strips C, B, and A. The lower horizontal line delimits approximately the depth of the specimen.

The results of this test indicate that 1- to 2-mm-wide cracks can be detected depending on the position and shape and on the moisture content of the specimen. Higher moisture content and more superficial cracks result in easier detection and interpretation of the received signal. Cracks less than 5 mm wide and at depths of 8 cm or more are difficult to distinguish from the signal's background noise. Hairline or sub-millimeter cracks cannot be identified with the current GPR technology.

**DRYING TESTS**

Tests were carried out in the laboratory using the GPR on a drying soil specimen contained within a cylindrical tray of 80 cm in diameter and 10 cm high. Clay, initially in a slurry state, was poured into the tray and left to dry in the laboratory-controlled environment (air relative humidity of approximately 60 % and temperature 24°C) during 36 days. The GPR device was used periodically to check for crack formation and propagation

8        *Geotechnical Testing Journal*
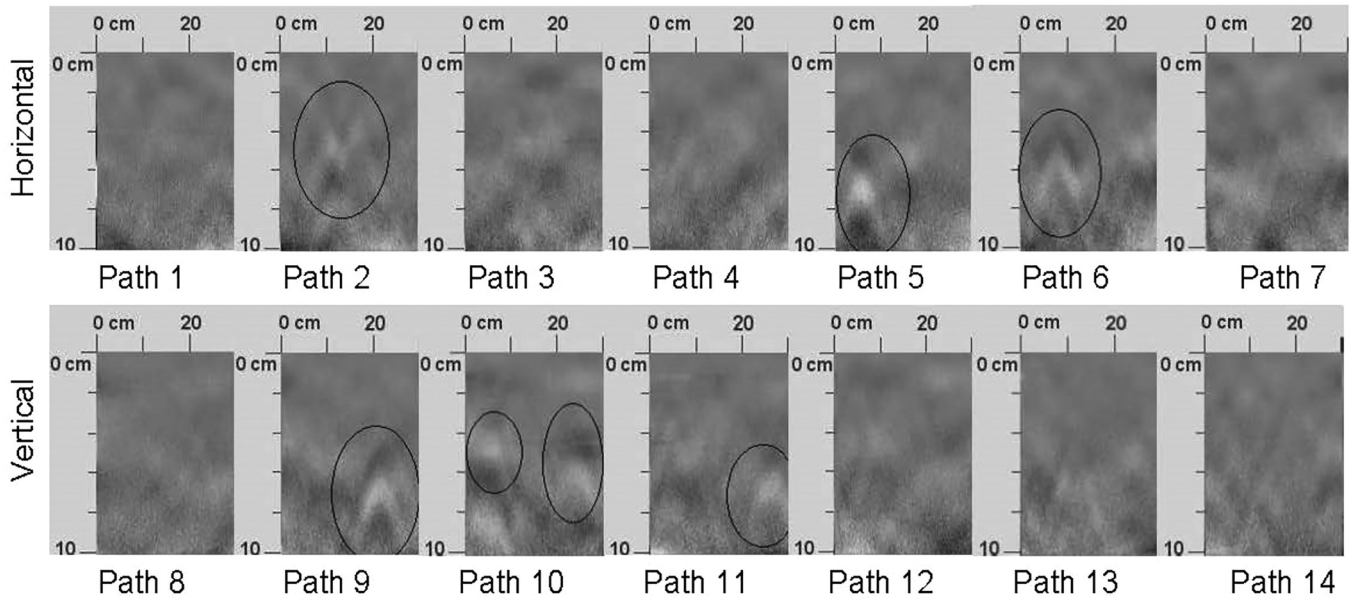
**FIG. 10**    GPR profiles on day 20.



**FIG. 11**

(a) suspected cracks on day 20 from GPR ($\Delta$ = bottom to top, $\odot$ = left to right), and (c,d) visible cracks on days 22, 28, and 36, respectively.
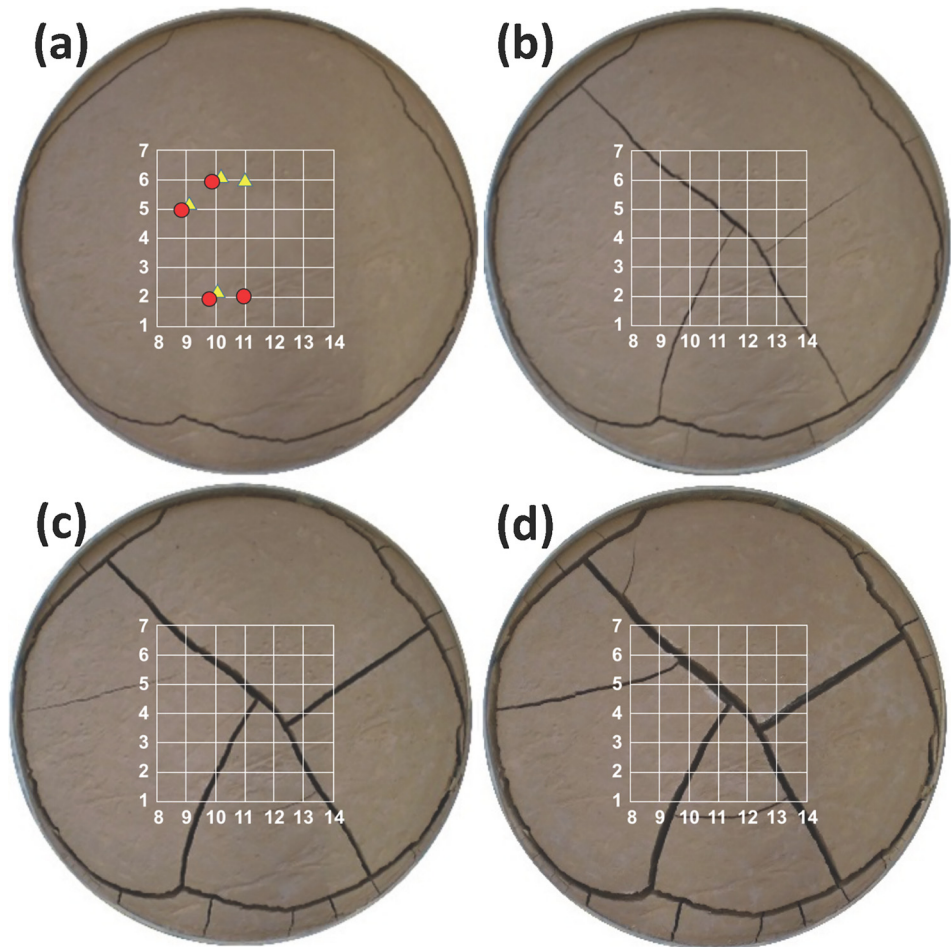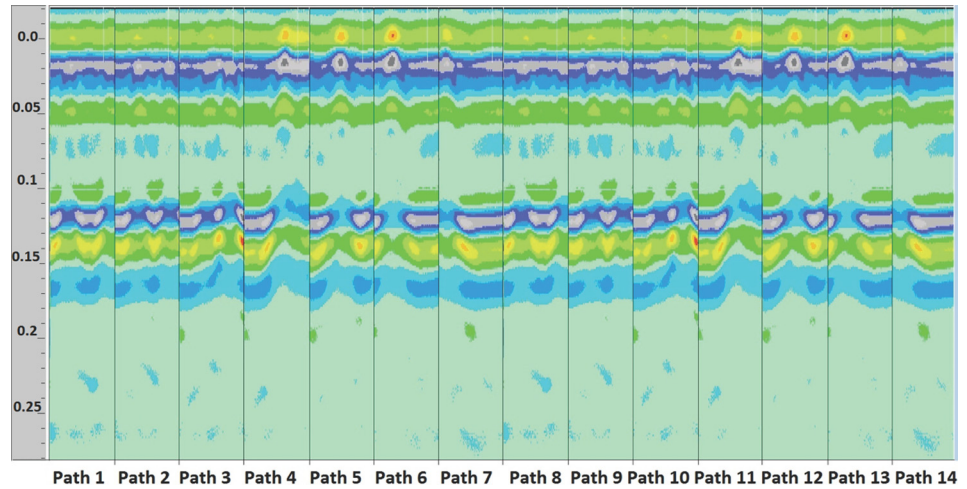
AQ4

**FIG. 12**

GPR profiles on day 22 from the 3D analysis using RADAN 6.6.



within the soil mass, and to calibrate the soil's electromagnetic properties. The use of the device requires a smooth, even surface on which it can slide. For that purpose, a 1-cm-thick poly(methyl methacrylate), or PMMA, circular plate was placed above the specimen.

A grid defining the line paths along which the device takes readings was affixed on top of the plate (see **Fig. 3**). The grid was shaped as a $30 \times 30$ cm$^2$ defining two sets of seven orthogonal traverses with a separation of 5 cm. Therefore, the soil portion of the specimen that was scanned by the GPR device was a square prism of dimensions $30 \times 30 \times 10$ cm$^3$, located at the center of the specimen. The nominal thickness of 10 cm, however, decreased during the drying process to 7 to 8 cm depending on the initial moisture content of the specimen. **Fig. 3** shows the initial stage of the soil inside the tray and the PMMA plate with the grid.

The GPR device allows for dielectric constant ($k$) values in the range of 4 to 12. The best results for the tests reported were obtained with a value of 12. The depth setting for scaling of the device is between 20 and 40 cm, the closest to the tests being 20 cm. Because the depth of the specimen was 10 cm, the results show an additional portion of 10 cm corresponding to the bottom boundaries of the testing equipment.

**Fig. 4** shows the evolution of the specimen subjected to desiccation during the 36 days that the test lasted. The figure shows that cracks developed sufficiently during the test to allow studying the capabilities of the device to detect cracks before they become visible.

The GPR device comes with simple post-processing software (StructureScan Mini viewer) that allows managing 2D graphical soil profiles from the data recorded, i.e., the result of the emission and subsequent collection of electromagnetic

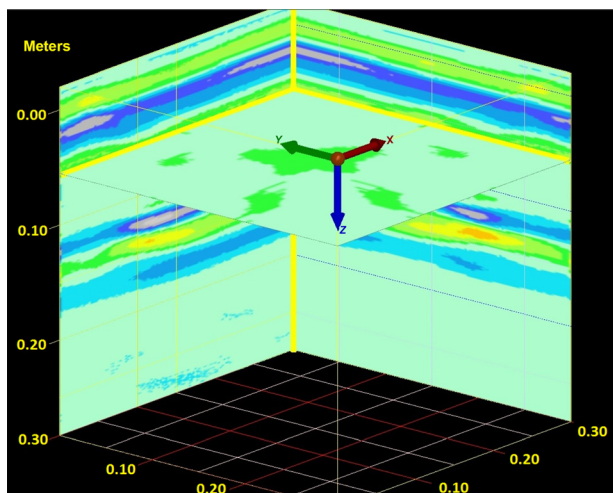**FIG. 13**   Pseudo 3D obtained by RADAN 6.6.



**FIG. 14**   Perpendicular profiles from RADAN 6.6 post-process.

10      *Geotechnical Testing Journal*



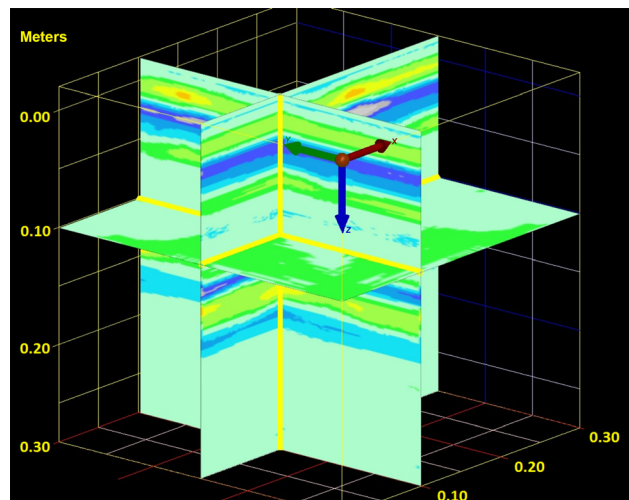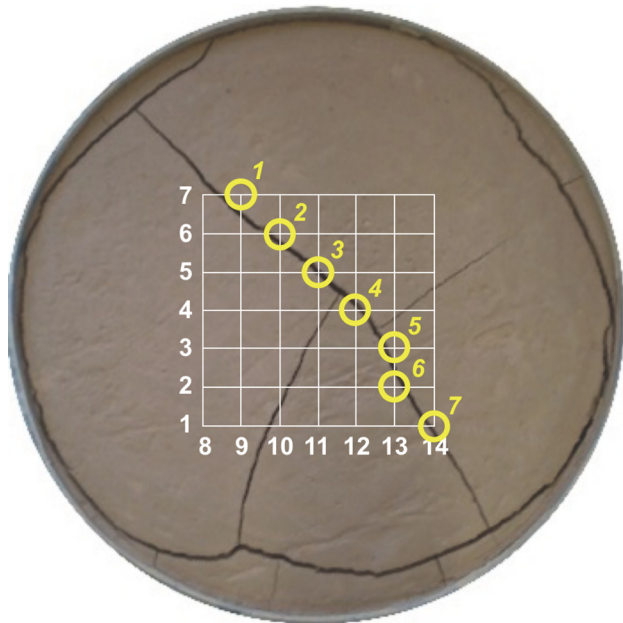**FIG. 15**   Intersections at which the pseudo-3D images are obtained.

waves reflections. Among other things, the program allows setting different values of the dielectric constant to better adjust to the medium and therefore match more accurately the actual dimensions of the specimen. It is known that soils between the dry and saturated states have a dielectric constant ranging from 20 to 30 (Alharti and Lange 1987; Bridge et al. 1996; Friedman 1997, 1998; Noborio 2001; Kim and Jeong 2004). Unfortunately, because the device used was made for scanning concrete and similar materials, it could only be set for dielectric constants between 4 and 12, which distorted the dimensions of the specimen under study, enlarging its thickness during the initial post-processing. This distortion is later adjusted with a more refined post-processing.

The evolution of the specimen along path 1 is shown in **Fig. 5**, with scans carried at days 1, 8, 15, 22, and 29 of the drying process. The sequence of images shows the expected gradual shrinkage of the specimen because of drying. Also, the profiles corresponding to days 22 and 29 contain a hyperbola that indicates the existence of an internal crack.

The profile corresponding to the first day of the test shows considerable heterogeneity. This was expected because specimens are initially in a disordered state because of the energy supplied during its fabrication and placement in the tray. Also, at this initial time, there is greater signal attenuation because the degree of saturation is at its maximum value. The handling of the specimen during the preparation stage may also contribute to cause areas or points on the soil mass capable of producing cracks during drying. The profile analyzed shows that this potential tends to disappear after the first few hours. After 24 h,

a thin layer of free water forms at the surface following initial settlement and homogenization of the specimen, and after the second day the profiles are considerably more homogeneous. The profiles corresponding to days 8 and 15 are fairly homogeneous suggesting that there are no internal cracks or significant heterogeneities in the area analyzed.

An important issue for obtaining meaningful information from GPR scans is learning how to detect an internal crack. **Fig. 6** shows the GPR profile along horizontal path 1 and the corresponding surface image obtained at day 21, where a visible surface crack intersecting path 1 can be associated to the hyperbola on the upper right corner of the GPR profile. On the other hand, the smaller quasi-vertical crack reaching, but not crossing, path 1 is not detected because it lies outside the influence zone of the GPR electromagnetic waves.

In contrast, **Fig. 7** shows the profile along path 1 and surface image 1 day later (day 22). The smaller crack has now propagated toward the center of the specimen, fully crossing the GPR path and therefore being detected, showing a clear new hyperbola on the upper left corner of the profile. Thus, it is clear that it is this diffraction pattern in the shape of a hyperbola that indicates the presence of a crack.

Further, **Fig. 8** shows the profile along path 3 and the surface image also at day 22 of the test. The intersection points of the two well-developed cracks with path 3 are closer than in path 1, resulting in two hyperbolas, which are also closer.

By measuring the distance between the tips of these hyperbolas the actual distance between the cracks can be known. Therefore, the analysis of the GPR profiles allows not only detecting the presence of cracks but also measuring the distance between them, with some limitations because of the precision of the device. This limitation is shown in **Fig. 9**, which shows the GPR profile along path 4 and surface image at day 22 of the test. Along this path, the cracks are separated 2.5 cm and the hyperbolas obtained with the GPR are nearly coincident in one large shape, as can be seen in the upper part of the profile, making the distinction between the two cracks impossible. The implication is that, with the current technology available, the precision does not allow discriminating between cracks that are closer than 5 cm. Another limitation is in the detection of very fine cracks. Cracks that are a few millimeters wide are easily detected but, in general, sub-millimeter cracks remain invisible to the GPR.

The post-processing software can show the graphical results of the tests using a variety of color schemes, which can be useful for better interpretation of the scans. The choice of a particular color scheme is a personal decision of the operator, who must choose it according to his/her own abilities in identifying the main features of the profile from the visual data. This ability must be trained to identify the main items, including cracks, that can be detected from the graphic results.

**FIG. 16**
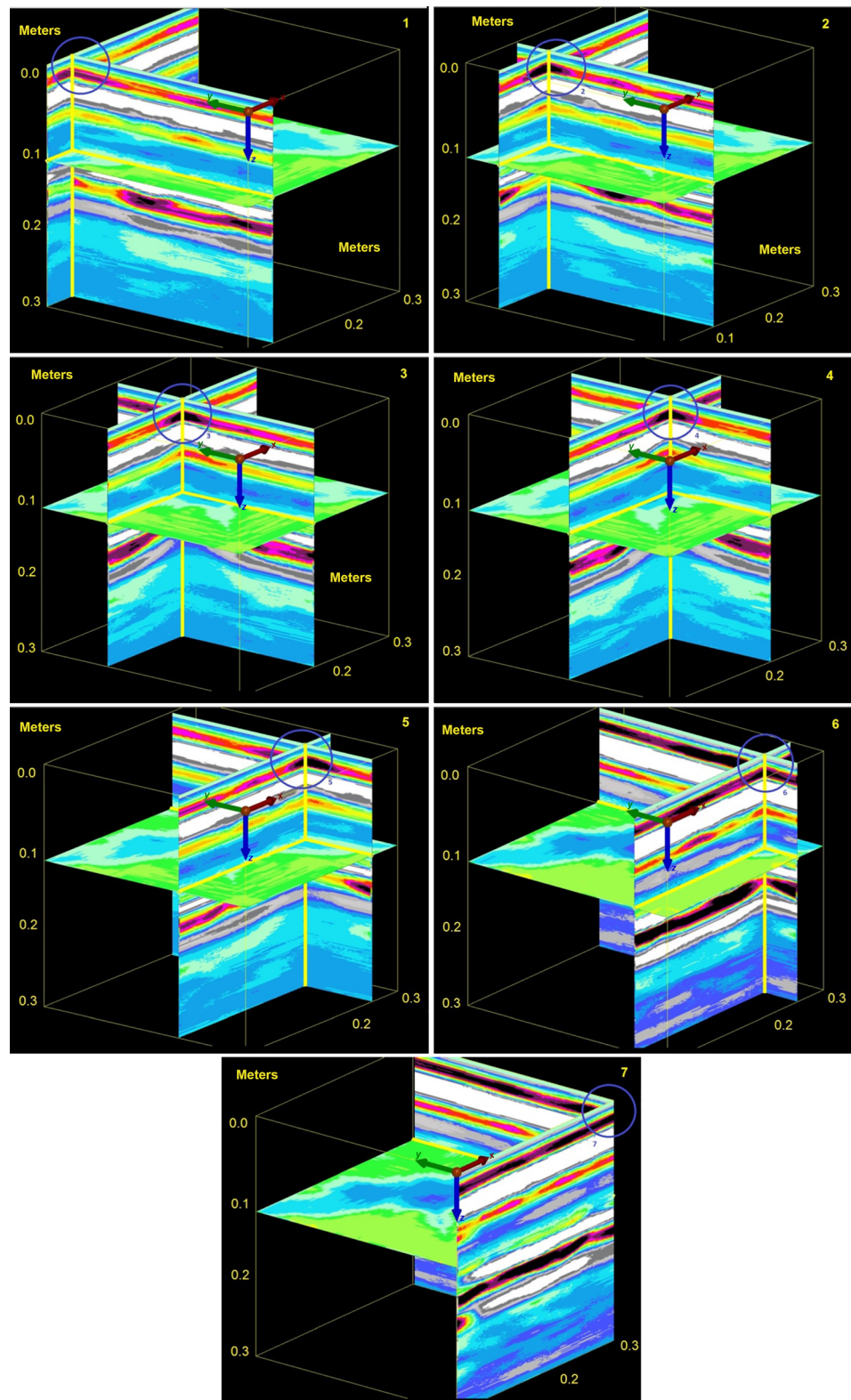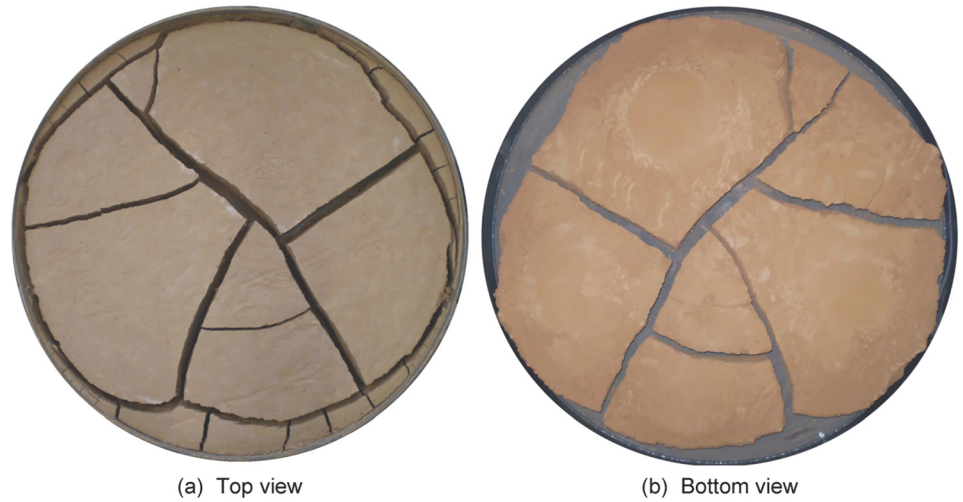
Pseudo-3D images at the intersections shown in **Fig. 15**.

12      *Geotechnical Testing Journal*

**FIG. 17**

Final crack patterns at the end of the test.



(a)  Top view                    (b)  Bottom view

442   The main objective of this technique is to detect the cracks
443   before they become visible. Therefore, it is necessary to check
444   the ability of the device to detect cracks that form at the bottom
445   or within the specimen before they appear on the surface. To
446   check for that, 14 profiles corresponding to day 20, before
447   cracks appeared on the surface of the specimen, were obtained
448   and analyzed. Of those, seven correspond to a horizontal
449   motion of the device (paths 1 to 7) and seven correspond to a
450   vertical motion (paths 8 to 14). **Fig. 10** shows those profiles on
451   which marks have been made on suspected points where cracks
452   might be progressing within the specimen. **Fig. 11a** shows the
AQ3 453   location of these suspected points in ~~plain~~ view on an image of
454   the specimen's surface after 20 days of drying. The circles indi-
455   cate suspected points detected during the horizontal motion of
456   the device (paths 1 to 7), whereas the triangles indicate

457   suspected points detected during the vertical motion (paths 8 to
458   14). Only in three of the suspected points there is coincidence
459   between the horizontal and vertical profiles and, interestingly, at
460   two of those points a crack appears at the surface 2 days later,
461   as seen in **Fig. 11b**, which shows the same surface on day 22 of
462   the test, with three cracks having become visible. The suspected
463   point located on paths 5/9 does not lead to a surface crack on
464   that day; however, on day 28 (**Fig. 11c**), a crack does appear on
465   the surface very close to this area, which then progresses to be
466   of a significant size on day 36 as seen in **Fig. 11d**.
467   A more detailed analysis of the results can be conducted
468   with the dedicated software RADAN (GSSI 2009), with
469   extended post-processing capabilities. As an example, **Fig. 12**
470   shows the 14 profiles corresponding to day 22 of the test in a
471   single view. The software allows the representation of two

**FIG. 18**

Instrumentation of the soil specimen for the cyclic test: (a) tensiometers T1–T6, Decagon sensors D1–D3; and (b) relative position of tensiometers at the end of the test.
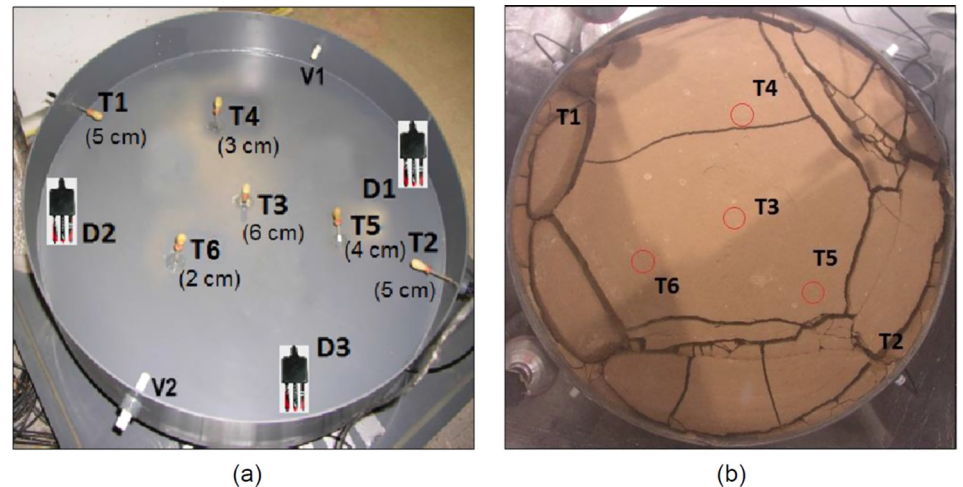


(a)                    (b)

**TABLE 4**   Specifications of temperature and relative humidity during the cyclic test.

| Stage | Duration (Days) | Temperature (°C) | Relative Humidity (%) |
|---|---|---|---|
| 1. First drying | 14 | 28 | 30 |
| 2. First wetting | 5 | 24 | 80 |
| 3. Flooding | 7 | 24 | 85 |
| 4. Second drying | 12 | 24 | 30 |
| 5. Second wetting | 17 | 22 | 75 |

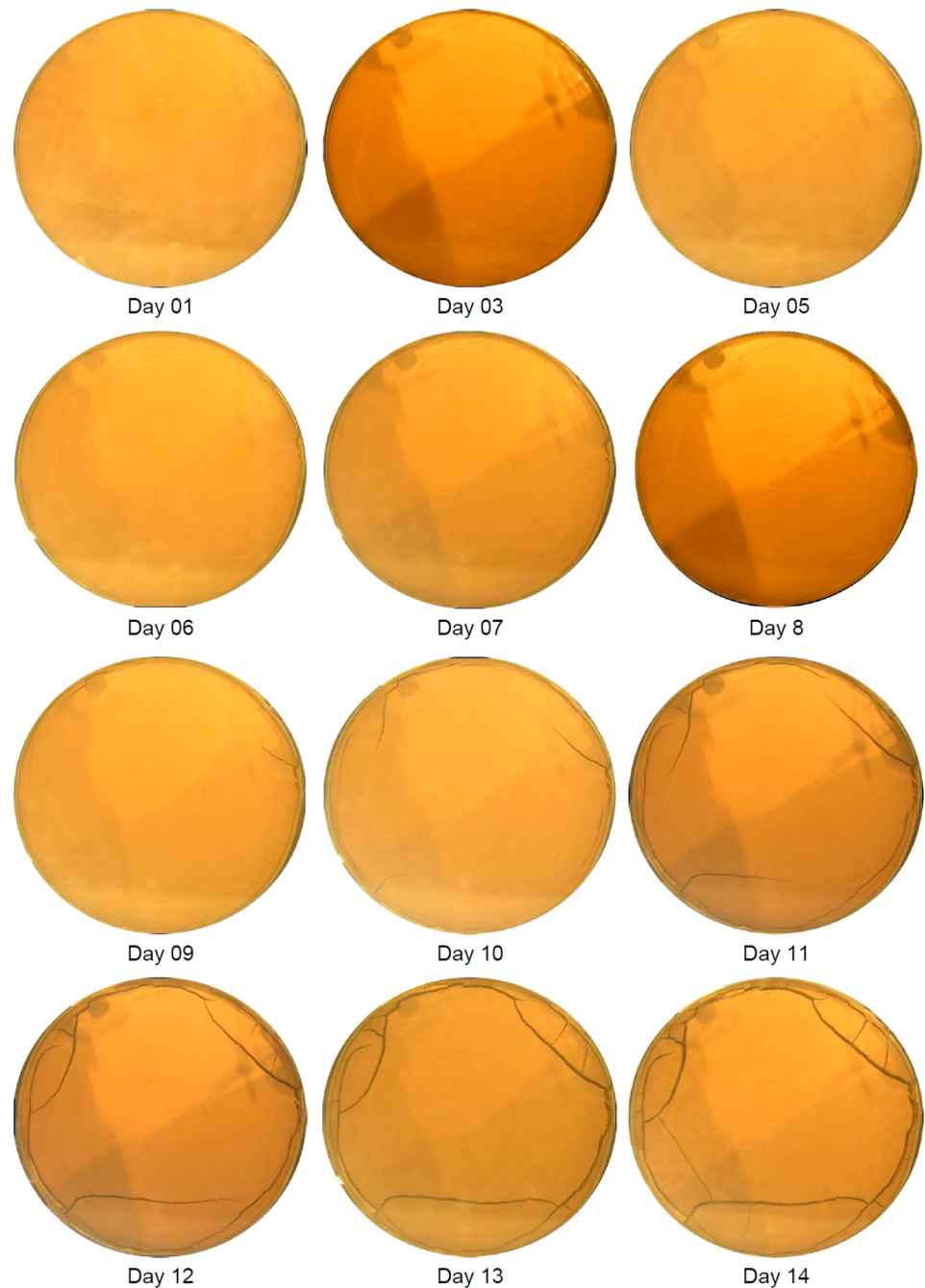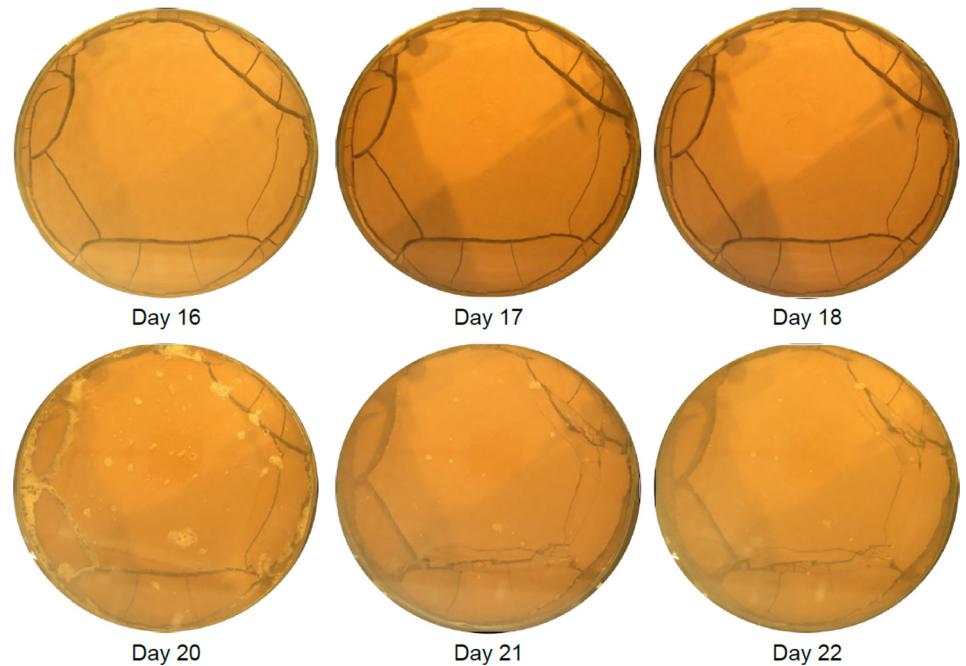**FIG. 19**

Sequence showing the first stage: first drying.

**FIG. 20**

Sequence showing the second and third stages: first wetting and flooding.



vertical orthogonal profiles and simultaneously, after post-processing, a horizontal slice at a chosen position to render a pseudo-3D view (**Fig. 13**).

**Fig. 14** shows two particular profiles corresponding to the $x$- and $y$-directions, with a horizontal slice. This particular construction can be used to analyze the cracking state at points situated in the intersection of the two profiles, at different depths. The quality and accuracy of the graphic results can be optimized by conveniently modifying the power gain as well as the input value of the dielectric constant.

As an example, focus is turned to the main crack that develops during the test (from the upper left to the bottom right corners). **Fig. 15** shows the crack and the points of interest where the pseudo-3D images will be generated. These images, at the seven intersection points, are shown in **Fig. 16**. The sequence shows that the crack path is detected easily from the pseudo-3D images. **Fig. 17** shows the final crack pattern at the end of the test as seen from the top (airside, left) and the bottom (after dismantling, right). The image of the bottom surface shows small cracks that have not emerged to the upper surface and have been invisible to the GPR because of their small width.

## CYCLIC TEST

This test consisted of five stages: first drying, first wetting, flooding, second drying, and second wetting, with a total duration of 55 days. It was carried out in an environmental chamber (Lakshmikantha 2009) that allows for temperature and humidity cycles (Levatti 2015). The specimen was a cylinder of 80 cm in diameter and 10 cm thick. It was fully instrumented (**Fig. 18**) with six tensiometers T5X (T1 to T6 in the figure) to record suction in the range 100 to $-200$ kPa, three sensors 5TE (D1 to D3 in the figure) to record soil temperature and volumetric water content, two Vaisala sensors (V1 and V2 in the figure) to record relative humidity and temperature of the soil, and three load cells to record weight changes because of changes in water content. **Table 4** shows the specifications of the temperature and relative humidity that were imposed during each stage of the test.

Images of the external surface were taken at regular intervals during the test. **Fig. 19** (first drying), **Fig. 20** (first wetting and flooding), **Fig. 21** (second drying), and **Fig. 22** (second wetting) show sequences of the evolution of the crack pattern on the surface of the specimen during the test. In addition to the instrument readings and the images of crack patterns, four GPR scans were made at 48, 167, 291, and 455 h during the first two stages of drying and wetting, to check for internal cracks before they were visible on the outer surface.

**Fig. 23** shows the evolution of the weight of the specimen (plus the container and instrumentation) with time during the five stages of the test. The spikes at days 3, 8, 13, and 20 correspond to the effect on the load cells of the GPR scans performed on those days, which are indicated in the figure.

## FIRST STAGE (FIRST DRYING, 14 DAYS)

The analysis of the weight changes recorded by the load cells shows that during the first stage approximately 12 L of water

**FIG. 21**
Sequence showing the fourth stage: second drying.



| Day 27 | Day 29 | Day 31 |
| Day 34 | Day 35 | Day 36 |
| Day 37 | Day 38 | Day 39 |
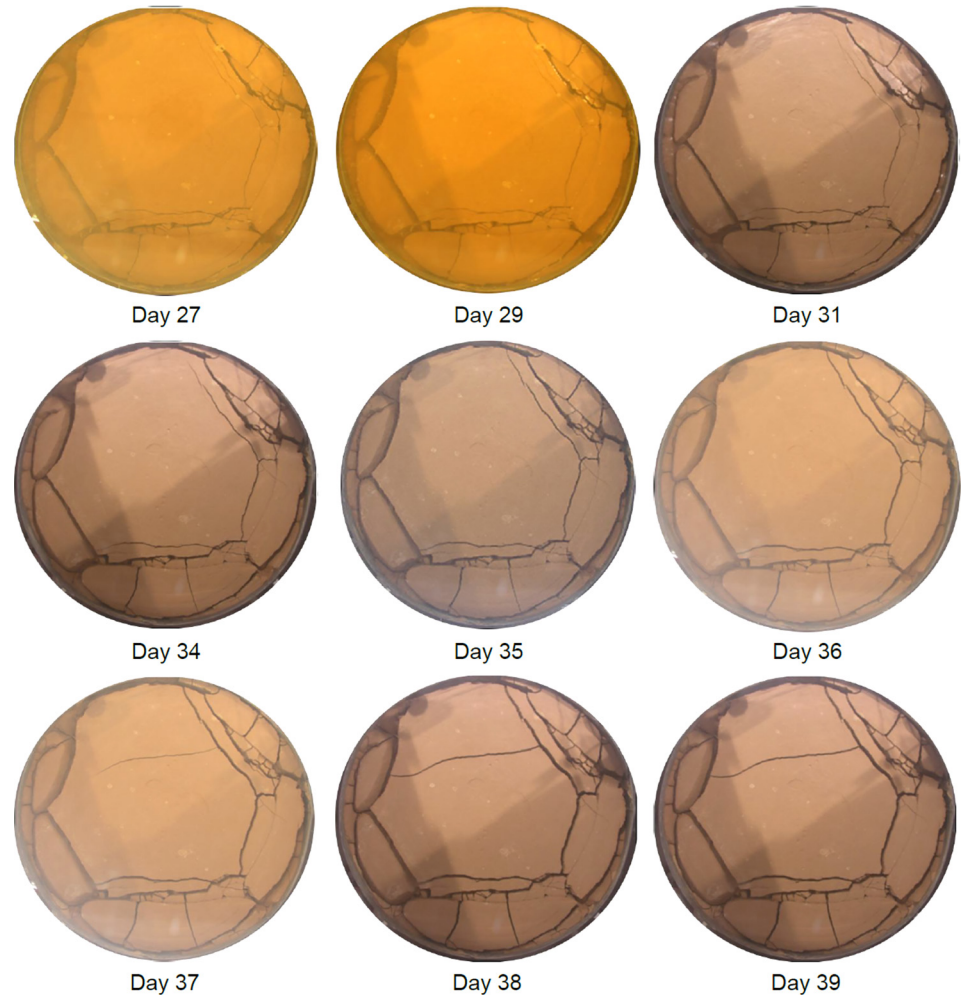
evaporated (**Fig. 23**). The same figure shows the times at which the GPR scans were conducted, clearly marked by an increase of weight detected by the load cells, and shows the temperature changes in the environmental chamber. During the first hours of the test, the temperature fluctuated until it reached a steady level of 28°C after about 2 days. From that time, the temperature inside the environmental chamber was kept at that level for the remainder of the test. No data from the sensors seems to point to the crack initiation or to their influence in the drying process (**Fig. 24**).
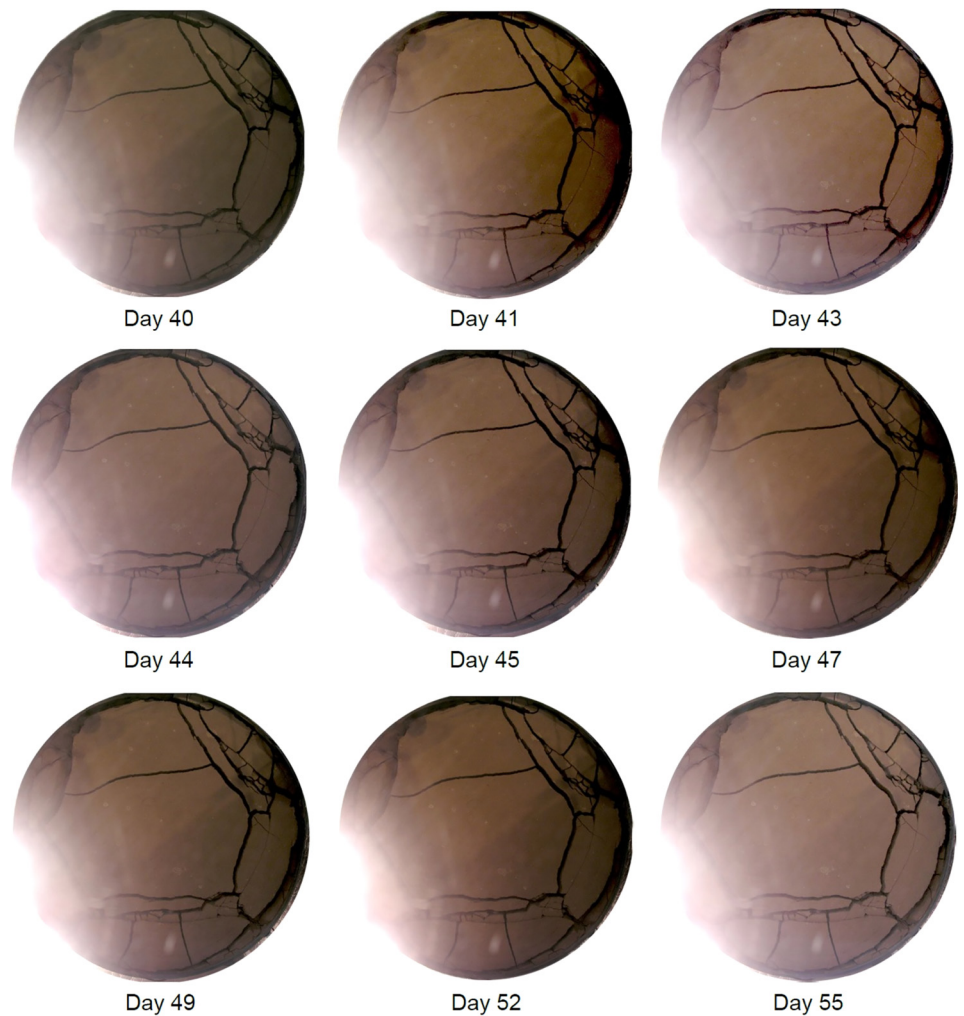
### SECOND STAGE (FIRST WETTING, 5 DAYS)

During this stage, the relative humidity of the chamber's atmosphere was raised to 80 %, while keeping the temperature constant at about 24°C. The reason for lowering the temperature from the previous level of 28°C was to check whether changing the air temperature changed significantly the soil temperature (**Fig. 25**).

**Fig. 26** shows an inflection point in the suction measurements from the tensiometers at the time when the chamber environment was changed. The slope, almost constant, is significantly less than during the previous drying stage. This proves that the tensiometers are capable of detecting these changes and therefore allow detection of environmental changes while measuring the soil's suction.

The objective of this wetting stage was to investigate how changing the chamber's air humidity affects suction. During the few days that this stage with high relative humidity lasted, no significant changes in the crack pattern were detected, regardless of the fact that the suction increased. During this stage, the loss of water in the specimen was almost negligible, showing equilibrium of water content between the soil and the environment; there seemed to be no interchange of water between the environment and the specimen. However, suction continued increasing, probably because of internal migration of water within the soil mass, or perhaps because of the slow response of the tensiometers.

16      *Geotechnical Testing Journal*

**FIG. 22**

Sequence showing the fifth stage: second wetting.



Day 40             Day 41             Day 43

Day 44             Day 45             Day 47

Day 49             Day 52             Day 55

562     During the stage, the recorded soil temperature shows a decrease that corresponds to the chamber's air temperature decrease (see **Figs. 24** and **25**), which indicates that the soil reaches thermal equilibrium with the air in a relatively short time of a few hours only.

**THIRD STAGE (FLOODING, 7 DAYS)**

568     The purpose of this stage was to simulate the impact of sudden intense precipitation on a cracked soil. To this effect, 9 L of water were added to the partially dry specimen. This was the volume of water the cracks and container capacity permitted and was 3 L short of the 12 L that were lost during the drying stage. This difference can be explained because of the extremely long time it would take to reintroduce the full 12 L of water into the soil pores. **Fig. 20** shows the flooded specimen at day 20.

576     During this stage, new cracks appeared, especially near the borders of cracks already present. This can be explained by the fact that, when flooding, the degree of saturation increases rapidly and the suction decreases accordingly, thus reducing the tensile strength and favoring the appearance of new cracks. The flooding conditions of humidity and temperature were maintained until no further changes of the crack pattern took place. The air relative humidity during this stage was kept at a constant 75 % (see **Fig. 24**).

**FOURTH STAGE (SECOND DRYING, 12 DAYS)**

585     The second drying stage was imposed with an air temperature of 24°C and relative humidity of 30 %. A comparison between the first and second drying stages shows that to reach a suction of 30 kPa 15 days were needed in the first stage, whereas only 10 days were needed in the second stage (see **Fig. 26**) even with a chamber temperature that was 4°C lower. Also, the rate of suction increase at the end of this second stage was constant and considerably higher.

594     The first part of these drying stages, in which the suction remains constant near 0 kPa, is shorter in the first of the drying

**FIG. 23**   Evolution of weight recorded with the load cells.
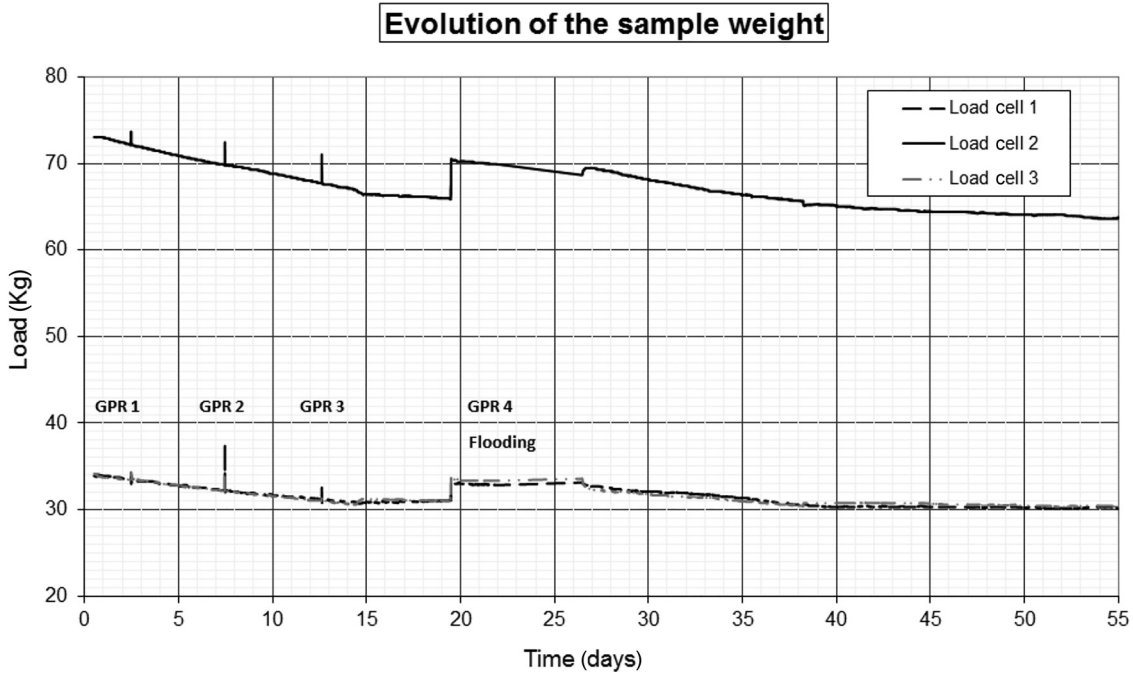


596  stages (7 days) than in the second (9 days). However, it must be
597  noted that in the first drying stage, the drying temperature and
598  humidity were imposed from the beginning, whereas in the
599  second drying stage there was a transition period with higher
600  air relative humidity. Another essential difference comes from
601  the fact that during the first drying, the specimen was fully
602  saturated from the beginning (all pores full of water), but in the
603  second stage, not all pores were full of water. Also, the specimen
604  at the start of the first drying stage did not have cracks, which is
605  not the case for this second stage.

606  An interesting fact is that because of flooding the specimen
607  experiences considerable degradation, with new cracks

**FIG. 24**   Evolution of air temperature and RH in the environmental chamber.
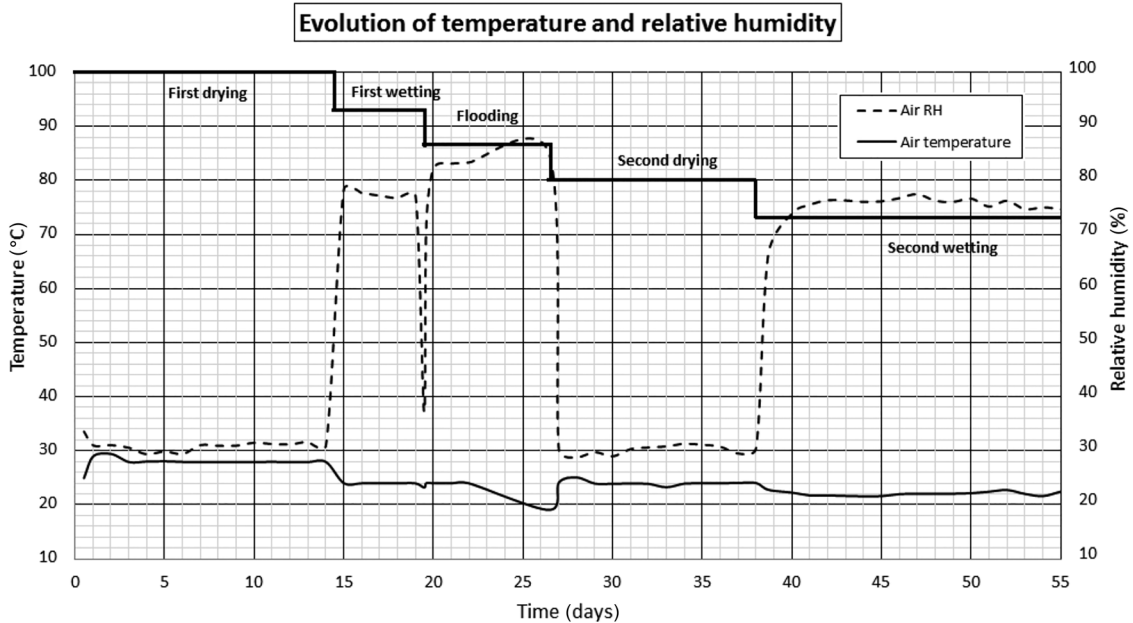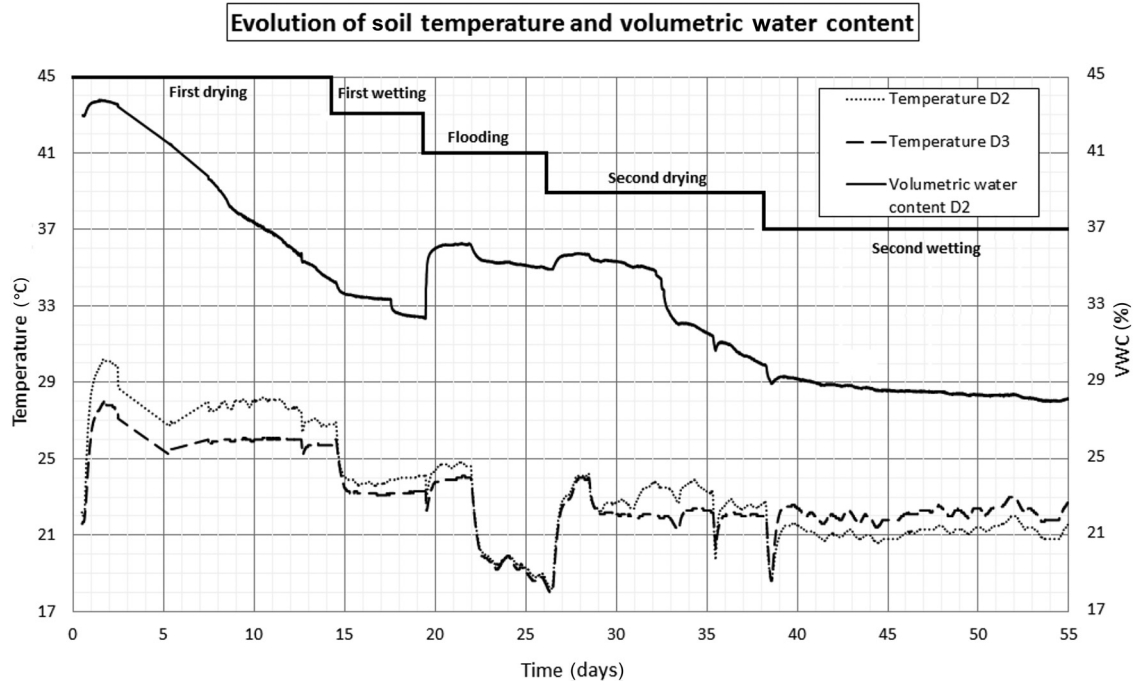
18      *Geotechnical Testing Journal*

**FIG. 25**    Evolution of soil temperature and volumetric water content recorded with sensors 5TE (D2 and D3 in **Fig. 18**).



developing close to the previous ones. This shows that cracking is irreversible at least for short time periods.

**610   FIFTH STAGE (SECOND WETTING, 17 DAYS)**

Once the specimen reached a dry condition more intense than in the first stage, the chamber relative humidity was raised again to 75 %, and the temperature was set to 22°C. These values were kept until the end of the 55 days. The readings of the tensiometers (**Fig. 26**) show how suction slowly decreases because of the new environmental conditions. **Fig. 25** shows how the specimen reaches thermal equilibrium, with decreasing soil temperature that approaches the air temperature.

**FIG. 26**    Evolution of suction recorded with tensiometers T5X (T1–T6 in **Fig. 18**).
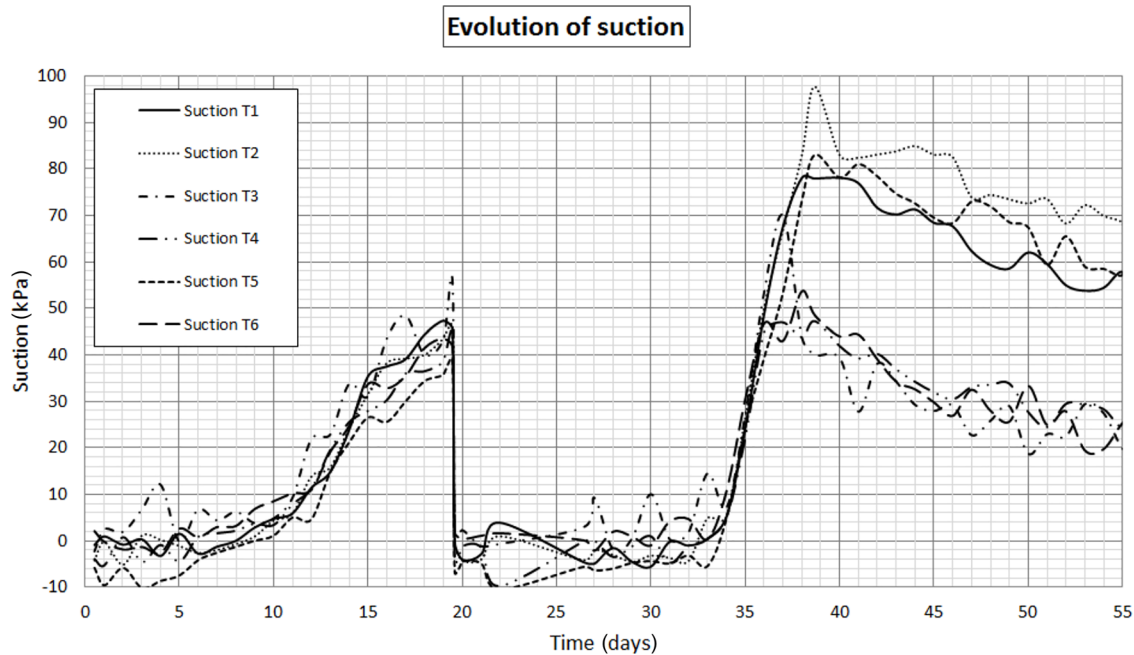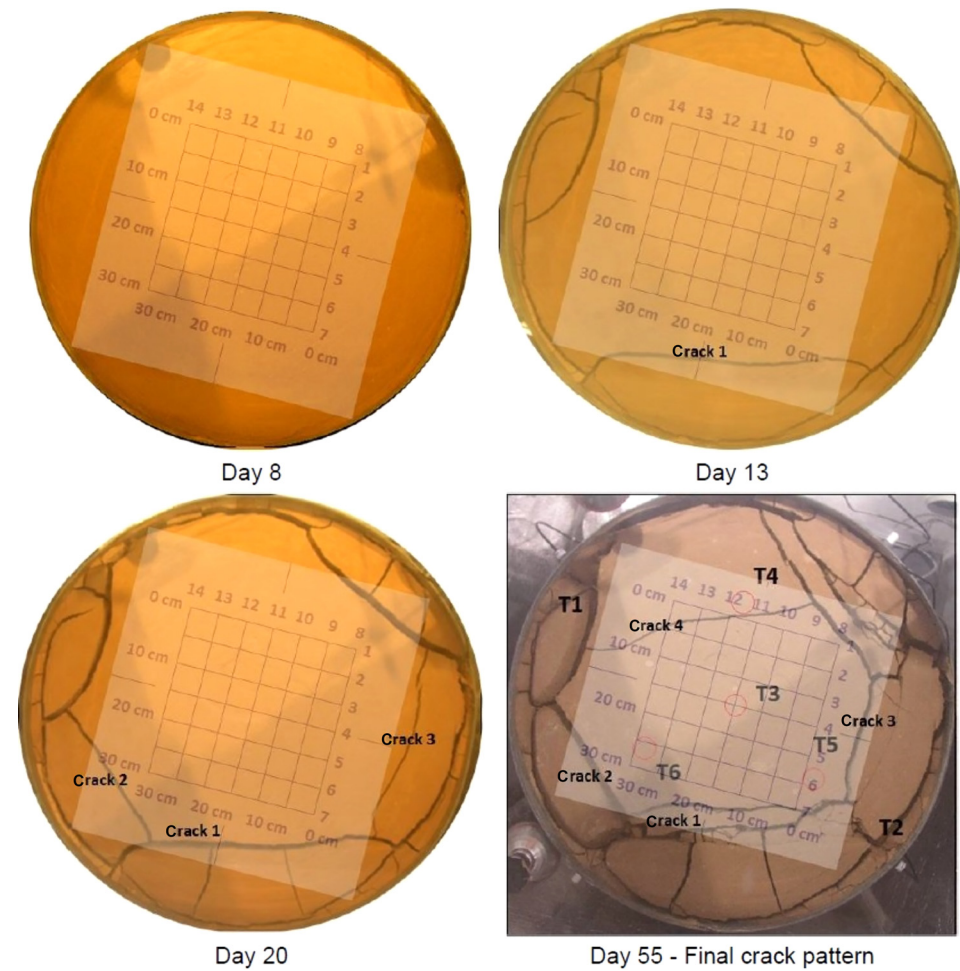
**FIG. 27**

Subsurface imaging of the specimen with GPR during the cyclic test.



Day 8

Day 13

Day 20

Day 55 - Final crack pattern

## GPR SCANS (DAYS 3, 8, 13, AND 20)

The GPR technique described in previous sections has been used to analyze the possible development of internal cracking during this test. The device has been able to detect the presence of the sensors at their respective position as well as other possible crack-initiating elements during the test.
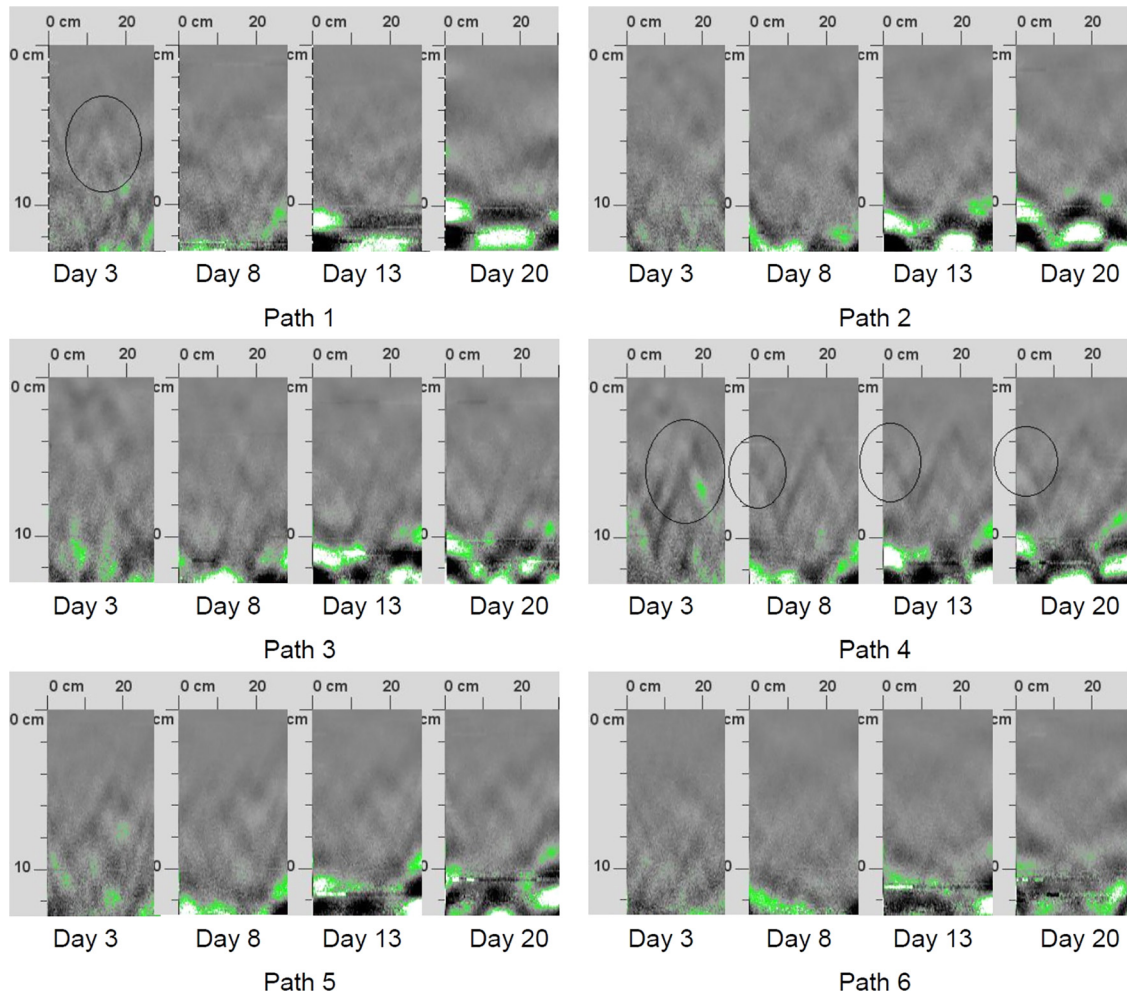
Fig. 27 shows the grid used during the days 3, 8, 13, and 20 to obtain the readings. The first visible crack on the top was produced on day 9 (Fig. 19); in consequence, the only information about internal cracks before day 9 comes from the GPR readings. The grid on days 13, 20, and at the final stage of the cyclic test (Fig. 27) permits establishing the relation within crack development and GPR profiles. Four cracks (crack 1, crack 2, crack 3, and crack 4), which appeared in chronological order during the drying stages, are identified to analyze the GPR readings. Fig. 28 (paths 1 to 6) and Fig. 29 (paths 7 to 14) show the GPR profiles obtained on days 3, 9, 13, and 20. Path 1 of day 3 shows, marked with a circle, what can be interpreted as a crack. However, this signal disappears in later profiles on days 8, 13, and 20. This was probably only a momentary discontinuity in the specimen's mass or a momentary heterogeneous distribution of water. Paths 2 and 3 show no cracks during the 4 days of auscultation. However, it is clear that the distribution of water is not totally homogeneous and the specimen's vertical shrinkage is detected as in the drying test (see previous section).

Path 4 shows clearly the central tensiometer T3 on the 4 days and a signal that can be interpreted as a crack at the beginning of the path, from day 3 onward. This crack can be the origin of crack 3 in Fig. 27 that is visible on the external surface of the specimen on day 16 (Fig. 20). Paths 5 and 6 show no cracks for each of the four GPR scans.

Path 7 (Fig. 29) shows a crack that evolves from the middle height of the specimen (day 3) close to the end of the path, propagating toward the surface (on day 20) that seems to be the origin of crack 2 in Fig. 27. Path 8 on day 20 shows crack 1, which on that day is already visible on the external surface of the specimen. Path 9 shows an internal crack that was not visible yet on the external surface. This crack evolved only partially from the bottom of the specimen and did not reach the external surface. Paths 10, 13, and 14 show no cracks for each of the four

20      *Geotechnical Testing Journal*

**FIG. 28**     Evolution of GPR profiles on paths 1–6 from day 3 to day 20.



Path 1

Path 2

Path 3

Path 4

Path 5

Path 6

GPR scans but the profiles show heterogeneity probable produced by the three tensiometers T3, T4, and T6, which were aligned with these paths. Path 11 shows the central tensiometer T3 and path 12 shows tensiometers T4 and T3 in the four GPR profiles, more clearly on day 3.

It is clear that the GPR is capable to detect the presence of the sensors. However, the presence of the sensors interferes with the main purpose of the GPR, which is to detect cracks. Therefore, it is recommended, if possible, to avoid placing sensors in the area where GPR scans will take place during testing.

## Conclusions

The ground-penetrating radar system described in this paper is a promising tool for non-destructive indirect detection of crack formation and propagation within a drying soil mass by allowing a more comprehensive monitoring of the internal cracks. The interpretation of the results is complex and requires acquired skill of the analyst, because the GPR use in soil cracking has to be adapted from its original, non-geotechnical,

purpose to the soil's particular characteristics, in particular to the fact that its electromagnetic properties do not remain constant over time because of the changes of its constituents. The ability of the analyst in identifying the main features of the cracking process from visual observation of the profiles is fundamental and requires considerable training involving not only visual ability, but also knowledge of the technical workings of the device and the software, so that adjustments can be made in all stages of the test: specimen design, definition of the scanner paths grid, and post-processing.

Regardless of some limitations, the GPR system is sensitive to changes in water content that occurs in the soil during desiccation. Cracks with crack width larger than 1 to 2 mm are easily detected, whereas thinner cracks are not identified with the currently available devices. The separation between cracks when the distance is more than about 5 cm can also be obtained from the GRP profiles. However, cracks that are closer than 5 cm create interferences in the profile, thus preventing the correct interpretation of the data. Given the continuous technical evolution of GRP devices, it is envisioned that with higher wave

**FIG. 29**   Evolution of GPR profiles on paths 7–14 from day 3 to day 20.
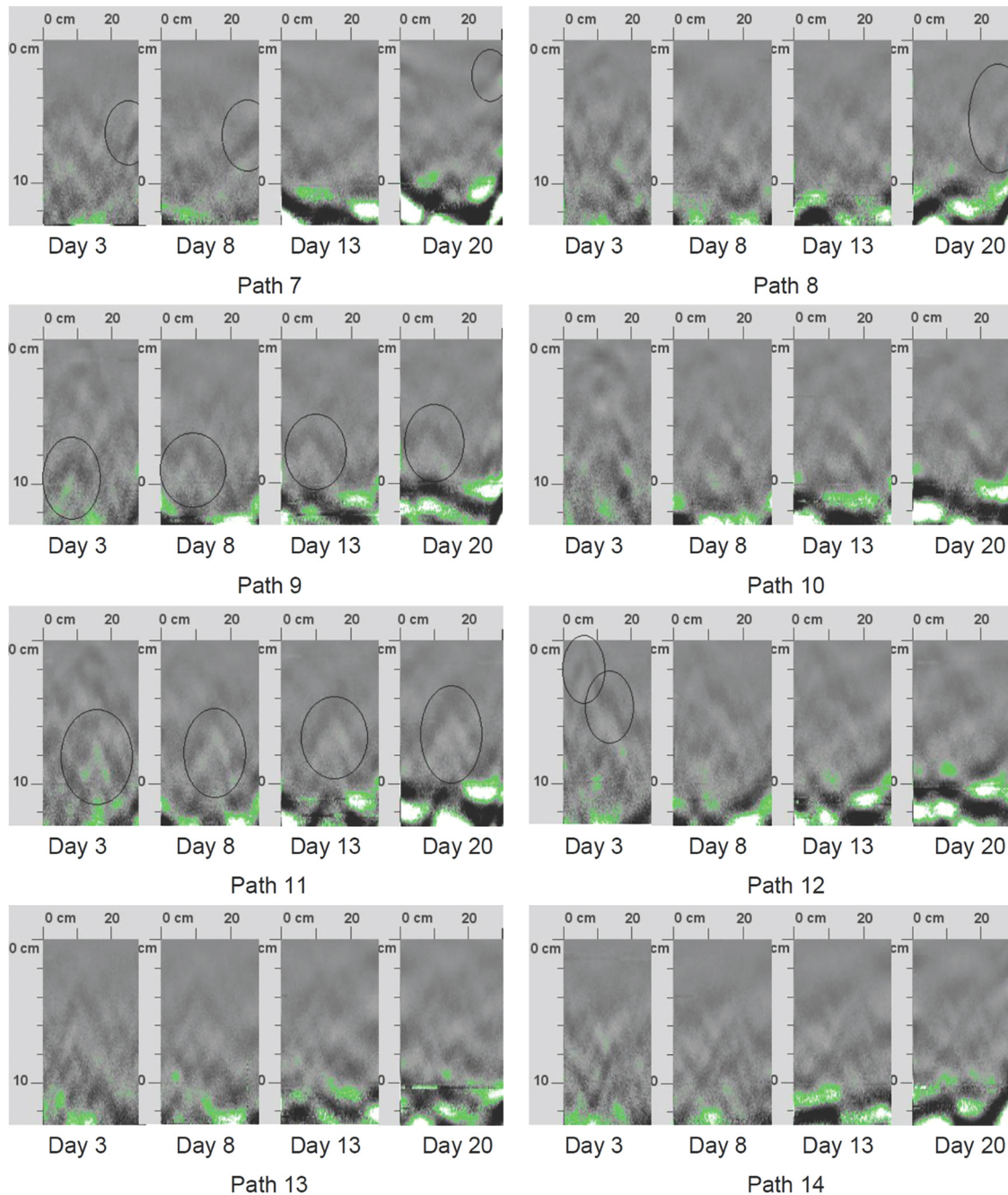


frequencies the resolution will improve significantly, thus allowing detection of thinner cracks and identification of the separation between them. For this to occur, of course, the industry must develop these higher-frequency devices, as the need for them increases and makes their development profitable.

A key advantage of the GPR technique is its low cost when compared to other systems such as X-rays, CT, scans or MRIs. The GPR device is much less expensive and fully portable. Its ease of use and continuous evolution makes it a good choice to work both in the field and in the laboratory and, when combined with currently available systems to study cracking in soils, can greatly improve the prediction and understanding of how shrinking of soils induce cracks, and how those cracks later propagate.

The cyclic test presented shows that cycles of wetting and flooding in addition to drying have a strong influence on the variables that govern the cracking phenomenon. Flooding produces additional cracks on the specimen, after drying and wetting, showing the irreversibility of cracking for the duration of the test.

22 *Geotechnical Testing Journal*

## 724 References

725 Alharti, A. and Lange, J., 1987, "Soil Water Saturation: Dielec-
726 tric Determination," *Water Resour. Res.*, Vol. 23, No. 4, pp.
727 591–595.

728 Ávila, G., 2004, "Estudio de la Retracción y el Agrietamiento de
729 Arcillas. Aplicación a la Arcilla de Bogotá," Ph.D. thesis,
730 Department of Geotechnical Engineering and Geosciences,
AQ7 731 Polytechnic University of Catalonia, Barcelona, Spain.

732 Barrera, M., 2002, "Estudio Experimental del Comportamiento
733 Hidro-Mecánico de Suelos Colapsables," Ph.D. thesis,
734 Department of Geotechnical Engineering and Geosciences,
735 Polytechnic University of Catalonia, Barcelona, Spain.

736 Brandes, I. M., 2005, "The Negative Chargeability of Clays,"
737 Ph.D. thesis, School of Civil and Environmental Engineering,
738 University of New South Wales, Sydney, Australia.

739 Bridge, B. J., Sabburg, J., Habash, K. O., Ball, J. A. R., and Han-
740 cock, N. H., 1996, "The Dielectric Behaviour of Clay Soils
741 and Its Application to Time Domain Reflectometry," *Austr.*
AQ8 742 *J. Soil Res.*, Vol. 34, pp. 825–835.

743 Chertkov, V. Y., 2002, "Modelling Cracking Stages of Saturated
744 Soils as They Dry and Shrink," *Eur. J. Soil Sci.*, Vol. 53, No.
745 1, pp. 105–118.

746 Cordero, J., Cuadrado, A., Ledesma, A., and Prat, P. C., 2014,
747 "Patterns of Cracking in Soils Due to Drying and Wetting
748 Cycles," *6th International Conference on Unsaturated Soils,*
749 *UNSAT 2014*, Sydney, Australia, Taylor & Francis, London,
AQ9 750 pp. 381–387.

751 Corte, A. and Higashi, A., 1960, "Experimental Research on
752 Desiccation Cracks in Soil," *Report No. 66*, Corps of Engi-
753 neers, U.S. Army Snow, Ice and Permafrost Research Estab-
754 lishment, Wilmette, IL.

755 Friedman, S. P., 1997, "Statistical Mixing Model for the Appar-
756 ent Dielectric Constant of Unsaturated Porous Media," *Soil*
757 *Sci. Soc. Am. J.*, Vol. 61, No. 3, pp. 742–745.

758 Friedman, S. P., 1998, "A Saturation Degree-Dependent Com-
759 posite Spheres Model for Describing the Effective Dielectric
760 Constant of Unsaturated Porous Media," *Water Resour. Res.*,
761 Vol. 34, No. 11, pp. 2949–2961.

762 GSSI, 2009, "RADAN Manual," Geophysical Survey Systems,
763 Salem, NH.

764 Haines, W., 1923, "The Volume-Changes Associated With
765 Variations of Water Content in Soil," *J. Agric. Sci.*, Vol. 13,
766 No. 3, pp. 296–310.

767 Hassan, A. and Toll, D. G., 2013, "Electrical Resistivity Tomog-
768 raphy for Characterizing Cracking of Soils," *Geo-Congress*
769 *2013*, American Society of Civil Engineers, Reston, VA,
AQ10 770 pp. 818–827.

771 Hu, L. B., Hueckel, T., Péron, H., and Laloui, L., 2008,
772 "Modeling Evaporation, Shrinkage and Cracking of Desic-
773 cating Soils," *IACMAG 12*, Goa, India, Indian Institute of
774 Technology, Mumbai, India, pp. 1083–1090.

775 Jahn, A., 1950, "Peculiar Polygonal Markings on the Meadows
776 in the Wieprz River Valley," *Acta Geol. Polonica*, Vol. 1,
777 No. 2, pp. 150–157.

778 Kim, M. I. and Jeong, G. C., 2004, "A Study on the Determina-
779 tion of Dielectric Constant of Saturated Porous Media Using
780 Frequency Domain Reflectometry System," *J. Eng. Geol.*,
781 Vol. 14, No. 2, pp. 179–187.

782 Knechtel, M. M., 1952, "Pimpled Plains of Eastern Oklahoma,"
783 *Bull. Geol. Soc. Am.*, Vol. 63, No. 7, pp. 689–700.

784 Knoll, M. D. and Knight, R., 1994, "Relationships Between
785 Dielectric and Hydrogeologic Properties of Sand-Clay
786 Mixtures," *Fifth International Conference on Ground Pene-
787 trating Radar*, Waterloo Centre for Groundwater Research,
788 Waterloo, Ontario, Canada, pp. 45–61. AQ11

789 Kodikara, J., Barbour, S. L., and Fredlund, D. G., 2000,
790 "Desiccation Cracking of Soil Layers," *Unsaturated Soils for*
791 *Asia*, Balkema, London, pp. 693–698.

792 Kodikara, J. K., Nahlawi, H., and Bouazza, A., 2004, "Modelling
793 of Curling in Desiccation Clay," *Can. Geotech. J.*, Vol. 41,
794 No. 3, pp. 560–566.

795 Lachenbruch, A. H., 1961, "Depth and Spacing of Tension
796 Cracks," *J. Geophys. Res.*, Vol. 66, No. 12, pp. 4273–4292.

797 Lakshmikantha, M. R., 2009, "Experimental and Theoretical
798 Analysis of Cracking in Drying Soils," Ph.D. thesis,
799 Department of Geotechnical Engineering and Geosciences,
800 Polytechnic University of Catalonia, Barcelona, Spain.

801 Lakshmikantha, M. R., Prat, P. C., and Ledesma, A., 2006, "An
802 Experimental Study of Cracking Mechanisms in Drying
803 Soils," *Environmental Geotechnics V*, Thomas, H. R., Ed.,
804 Thomas Telford, London, pp. 533–540.

805 Lakshmikantha, M. R., Prat, P. C., and Ledesma, A., 2009,
806 "Image Analysis for the Quantification of a Developing
807 Crack Network on a Drying Soil," *Geotech. Test. J.*, Vol. 32,
808 No. 6, pp. 505–515.

809 Lakshmikantha, M. R., Prat, P. C., and Ledesma, A., 2012,
810 "Experimental Evidences of Size-Effect in Soil Cracking,"
811 *Can. Geotech. J.*, Vol. 49, No. 3, pp. 264–284.

812 Lakshmikantha, M. R., Prat, P. C., and Ledesma, A., 2013a,
813 "Evidences of Hierarchy in Cracking of Drying Soils," *ASCE*
814 *Geotechnical Special Publication*, Vol. 231, American Society
815 of Civil Engineers, Reston, VA, pp. 782–789.

816 Lakshmikantha, M. R., Reig, R., Prat, P. C., and Ledesma, A.,
817 2013b, "Origin and Mechanism of Cracks Seen at the Bot-
818 tom of a Desiccating Soil Specimen," *ASCE Geotechnical*
819 *Special Publication*, Vol. 231, pp. 790–799.

820 Lakshmikantha, M. R., Prat, P. C., and Ledesma, A., 2016,
821 "Desiccation of Thin Soil layers: Effect of Boundary Con-
822 ditions," *Geoderma* (submitted). AQ12

823 Lambe, T., 1958, "The Structure of Compacted Clay," *J. Soil*
824 *Mech. Found. Div.*, Vol. 84, No. 2, pp. 1–34. AQ13

825 Lau, J. T. K., 1987, "Desiccation Cracking of Clay Soils," M.S.
826 thesis, Department of Civil Engineering, University of
827 Saskatchewan, Saskatoon, Saskatchewan, Canada.

828 Levatti, H. U., 2015, "Estudio Experimental y Análisis Numérico
829 de la Desecación en Suelos Arcillosos," Ph.D. thesis, Depart-
830 ment of Geotechnical Engineering and Geosciences, Poly-
831 technic University of Catalonia, Barcelona, Spain.

832 Longwell, C. R., 1928, "Three Common Types of Desert Mud
833 Cracks," *Am. J. Sci.*, Vol. 15, No. 86, pp. 136–145.

834 Mitchell, J. K., 1993, *Fundamentals of Soil Behaviour*, Wiley,
835 New York.

Morris, P. H., Graham, J., and Williams, D. J., 1992, "Cracking in Drying Soils," *Can. Geotech. J.*, Vol. 29, No. 2, pp. 263–277.

Morrison, F. and Gasperikova, E., 2015, "The Berkeley Course in Applied Geophysics," The University of California, Berkeley, CA.

Mukunoki, T., Otani, J., Maekawa, A., Camp, S., and Gourc, J. P., 2010, "Investigation of Crack Behavior on Cover Soils at Landfill Using X-Ray CT," *Advances in X-Ray Tomography for Geomaterials*, Desrues, J., Viggiani, G., and Bésuelle, P., Eds., Wiley, New York, pp. 213–219.

Nahlawi, H. and Kodikara, J., 2006, "Laboratory Experiments on Desiccation Cracking of Thin Soil Layers," *Geotech. Geol. Eng.*, Vol. 24, No. 6, pp. 1641–1664.

Noborio, K., 2001, "Measurement of Soil Water Content and Electrical Conductivity by Time Domain Reflectometry: A Review," *Comput. Electr. Agric.*, Vol. 31, No. 3, pp. 213–237.

Otani, J. and Obara, Y., 2004, *X-Ray CT for Geomaterials: Soils, Concrete, Rocks*, Swets & Zeitlinger, Lisse, The Netherlands.

Pérez, V., 2001, "Radar de Subsuelo. Evaluación para Aplicaciones en Arqueología y en Patrimonio Histórico-Artístico," Ph.D. thesis, Polytechnic University of Catalonia, Barcelona, Spain.

Péron, H., Hueckel, T., Laloui, L., and Hu, L. B., 2009, "Fundamentals of Desiccation Cracking of Fine-Grained Soils: Experimental Characterisation and Mechanisms Identification," *Can. Geotech. J.*, Vol. 46, No. 10, pp. 1177–1201.

Prat, P. C., Ledesma, A., Cuadrado, A., and Levatti, H. U., 2013, "Ground Penetrating Radar System for Detection of Desiccating Cracks in Soils," *ComGeo-III*, International Centre for Computational Engineering, Kraków, Poland, pp. 249–258.

Rodríguez, R. L., Sánchez, M. J., Ledesma, A., and Lloret, A., 2007, "Experimental and Numerical Analysis of a Mining Waste Desiccation," *Can. Geotech. J.*, Vol. 44, No. 6, pp. 644–658.

Samouëlian, A., Cousin, I., Richard, G., Bruand, A., and Tabbagh, A., 2003, "Electrical Resistivity Imaging for Detecting Soil Cracking at the Centimetric Scale," *Soil Sci. Soc. Am. J.*, Vol. 67, No. 5, pp. 1319–1326.

Simpson, W. E., 1936, "Foundation Experience With Clay in Texas," *Civil Eng.*, Vol. 4, No. 1, pp. 581–584.

Skempton, A. W. and Northey, R. D., 1952, "The Sensitivity of Clays," *Géotechnique*, Vol. 3, No. 1, pp. 100–106.

Tang, C.-S., Shi, B., Liu, C., Gao, L., and Inyang, H., 2011, "Experimental Investigation of the Desiccation Cracking Behavior of Soil Layers During Drying," *J. Mater. Civil Eng.*, Vol. 23, No. 6, pp. 873–878.

Vogel, H. J., Hoffmann, H., and Roth, K., 2005, "Studies of Crack Dynamics in Clay Soil. I: Experimental Methods, Results and Morphological Quantification," *Geoderma*, Vol. 125, Nos. 3–4, pp. 203–211.

White, W. A., 1961, "Colloid Phenomena in Sedimentation of Argillacious Rocks," *J. Sediment. Petrol.*, Vol. 31, No. 4, pp. 560–570.

Willden, R. and Mabey, D. R., 1961, "Giant Desiccation Fissures on the Black Rock and Smoke Creek Deserts, Nevada," *Science*, Vol. 133, No. 3461, pp. 1359–1360.